A Nacreous Self-Assembled Nanolaminate for Corrosion Resistance on 2024-Al Alloy

Matthew Gordon

Thesis submitted to the Faculty of the Virginia Polytechnic Institute and State University
in partial fulfillment of the requirements for the degree of

Masters of Science
In
Materials Science and Engineering

Dr. Sean Corcoran
Dr. Richey Davis
Dr. Bill Reynolds
Dr. Ronald Kander

May 24, 2001
Blacksburg, Virginia Tech

Keywords: ISAM, ESAM, AFM, biomimetic, Ultem, polyelectrolyte, aluminum, chromate conversion coating, self assembly

A Nacreous Self-Assembled Nanolaminate
for Corrosion Resistance on 2024-Al Alloy

Matthew Gordon

ABSTRACT

Nanometer thick layers of clay and polymer were formed on mica, silicon, and aluminum 2024-T3 alloy using alternating solutions of positively and negatively charged polymer and clay, respectively. Atomic force microscopy was used to observe the morphology of the composite films on mica and silicon. It was found that solution concentrations of clay above 0.02 weight percent lead to the uncontrolled deposition of clay platelets on the substrate's surface. By using solution concentrations of clay above 0.02 weight percent and ultrasonic agitation together it is possible to deposit a uniform monolayer of clay platelets on a mica substrate in ≤ 20 seconds. Ultrasonic agitation also produced crude patterns of montmorillonite platelets.

Thin films of poly(diallydimethylammonium chloride) (PDDA) were made using concentrations ≥ 2 weight percent of PDDA. It was found that the PDDA formed several unusual morphologies. Spherulites of PDDA were observed with AFM and the glass transition temperature of high molecular weight PDDA was measured using differential scanning calorimetry (DSC).

Circular regions of positive charge were discovered on silicon wafers provided by three different sources. These areas of charge have never been reported in literature, but can easily be detected by placing wafers into solutions containing negatively or positively charged solutions of clay or polymer, respectively. The exact nature of these charged regions is unknown, but it is hypothesized that impurities on silicon wafers create the circular regions of positive charge.

ISAM films made of a polyamide salt and a synthetic clay, Laponite RD®, demonstrated significant corrosion resistance on 2024-T3 Al alloys after 168 hours of salt spray testing. The ISAM films offered corrosion protection only if there was a significant layer of underlying surface oxide present, however. It was found that ISAM deposited films of polyarylic acid (PAA) and polyallylamine hydrochloride (PAH) may offer some corrosion resistance on 2024-T3 Al alloys, but these films' corrosion resistance is severely hampered by the presence of Cl^- in the PAH solution.

Funding from this project was gratefully received from the Materials Science and Engineering Department at Virginia Tech; Luna Innovations Inc; the American Chemical Society / Petroleum Research Fund #34412-G5 and the Environmental Protection Agency Contract #68-D-00-244.

ACKNOWLEDGEMENTS

I'd like to thank a number of the people profusely for helping me to complete my thesis. Brian Okerburg for teaching me how to run the AFM. David Brooks for getting a nitrogen supply hooked up to the furnace in Kander's lab. Ekram Abbas for running a lot of salt spray test samples, often on short notice. Mike Miller for supplying me with funding, resources and a project. Dr. Topasna and Dr. Davis for their invaluable knowledge of ISAM. Dr. Hendricks and David Gray for supplying me with silicon and giving me advice on the "crop circles". Dr. Reynolds and Dr. Kander for being on my defense committee. Dr. Rick Clark for giving me access to Luna's labs and a chance to do some unorthodox research and last, but certainly not least, Dr. Corcoran for advising me and supplying me with additional funding when the EPA contract ran out.

TABLE OF CONTENTS

TABLE OF FIGURES

LIST OF TABLES

CHAPTER 1: GENERAL INTRODUCTION

High strength aluminum alloys, such as 2024-T3 Al, are widely used in the aerospace industry for their combination of mechanical properties and low density, however these same alloys usually exhibit poor corrosion resistance. A number of corrosion protection schemes are currently used to protect 2024-T3 Al alloys, the most successful of which are chromate conversion coatings (CCCs). Unfortunately, CCCs also contain highly toxic hexavalent chromium. As a result of their toxicity, there is increasing pressure from environmental legislation to find more environmentally benign alternatives to CCCs

The subject of this thesis is to utilize thin films produced by ionized self-assembled monolayer (ISAM) technology to produce environmentally friendly corrosion resistant coatings on 2024-Al alloys. ISAM coatings consist of nanometer thin layers of water-soluble polyelectrolytes and nanoparticles. To date, only one corrosion resistant coating made using ISAM has appeared in literature. In addition to offering corrosion protection to their substrates, corrosion resistant coatings must also be mechanically durable enough to survive their environment. For this reason, it was determined that one of the ISAM coatings' layers should be made from nanometer thin clay platelets to simulate nacre, the biological microstructure found in mollusk shells that give mollusks shells their outstanding mechanical properties.

This thesis is subdivided into three chapters. Chapter 1 of this thesis overviews ISAM, clays, nacre and ISAM films made using montmorillonite clays and poly(diallyldimethylammonium chloride). Chapter 2 covers unusually morphologies of PDDA, montmorillonite, and Laponite RD® clays that were observed. Chapter 3 discusses the actual application of ISAM corrosion resistant coatings on a 2024-Al and their performance under salt spray testing.

CHAPTER 2: MONTMORILLONITE FILMS

A. Introduction

1. Description of the ISAM Process

The proposed nanolaminate will be processed using ISAM technology. During an ISAM process, a charged substrate, such as, but not limited to: silicon wafers, glass slides, plates of mica, or sheets of polyethyleneterephthalate (PET) are dipped into an aqueous solution of oppositely charged molecules.[1] The molecules in solution adhere to the surface of the substrate and reverse the sample's surface charge. Once the surface of the substrate is saturated with oppositely charged molecules it is cleaned in deionized water to remove any loosely bound molecules. Then the sample is dipped into a solution filled with molecules charged opposite of the sample's surface. Columbic attractions adhere these molecules to the sample's surface; the sample is then washed with deionized water again and the process is repeated. Figure 2.1 gives a diagram of the process, which can be repeated indefinitely. Typical deposition times found in literature range between five to ten minutes per layer. No analytical or numerical models of ISAM deposition rates exist yet.

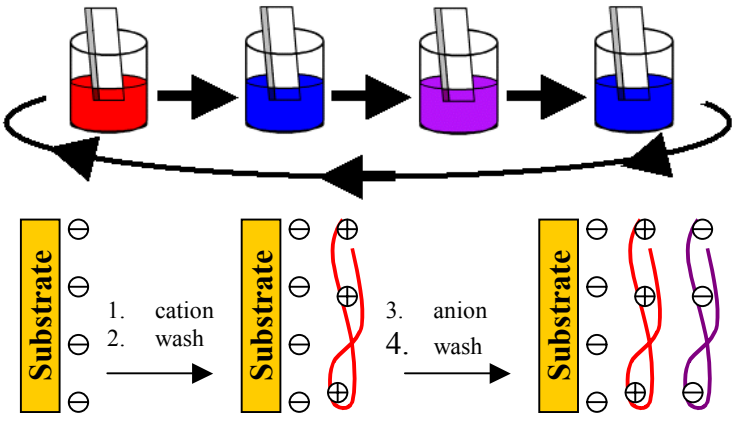

[1] Gero, Decher. "Fuzzy Nanoassemblies: Toward Layered Polymeric Multicomposites." Science. v377, p1232, Aug 29, 1997.

Figure 2.1: ISAM process with polycation / polyanion pair

In theory, there are "no restrictions with respect to substrate size and topology; multilayers have been prepared on colloids and on objects with dimensions of several tens of centimeters."[2] ISAM has been used to deposit polyelectrolytes, charged nano-particles, proteins, clays, and even viruses.[2-8] Research at Virginia Tech, often in conjunction with Luna Innovations Inc, has been done to identify potential applications of ISAM films as photovoltaics, light emitting diodes and non-linear optics.[9-13] In addition, ISAM films have demonstrated mechanical stability after being heated to 150^{o}C. [14]

---

[2] Sano et al. "Formation of Ultrathin Polymer Layers on Solid Substrates by Means of Polymerization-Induced Epitaxy and Alternate Adsorption." Annual Review Material Science. v26, p153, 1996.

[3] Decher, G; Schmitt, J. "Fine-Tuning of film thickness of ultrathin multiplayer films composed of consecutively Alternating Layers of Anionic and Cationic polyelectrolytes." Progress in Colloid & Polymer Science. v89, p160, 1992.

[4] Clark, Sarah L; Montague, Martha F; Hammond, Paula T. "Selective Deposition in Multilayer Assembly: SAMs as Molecular Templates." Supramolecular Science. v4, n1-2, p141, 1997.

[5] Clark, Sarah L; Montague, Martha F; Hammond, Paula T. "Ionic Effects on Sodium Chloride on Templated Deposition of Polyelectrolytes Using Layer-by-Layer Ionic Assembly." Macromolecules. v30, p7237, 1997.

[6] Polyelectroylte Adsorption Process Characterized in Situ using the Quartz Crystal Microbalance Technique: Alternate Adsorption Properties in Ultrathin Polymer Films." Colloids and Surfaces A: Physicochemical and Engineering Aspects. v173, p39, 2000.

[7] Tsukruk, V.V. et al. "Electrostatic Deposition on Polyionic Monolayers on Charged Surfaces." Macromolecules. v30, p6615, 1997.

[8] Cooper, Thomas M. et al. "Preparation of Polypeptide-Dye Multilayers by an Electrostatic Assembly Process." Materials Research Symposium Proceedings. v351, p239, 1994.

[9] C. Figura, P.J. Neyman, D. Marciu, C. Brands, M.A. Murray, S. Hair, R.M. Davis, M.B. Miller, and J.R. Heflin." Thermal Stability and Immersion Solution Dependence of Second Order Nonlinear Optical Ionically Self-Assembled Films." SPIE Proc. v3939, p214, 2000.

[10] C. Figura, P.J. Neyman, D. Marciu, C. Brands, M.A. Murray, S. Hair, M.B. Miller, R.M. Davis, and J.R. Heflin. "Control of Second-Order Nonlinear Optical Susceptibility in Ionically Self-Assembled Films by pH and Ionic Strength." Materials Research Society Symposium Proceedings, v506, 1999.

[11] D. Marciu, M.B. Miller, J.R. Heflin, M.A. Murray, A.L. Ritter, P.J. Neyman, W. Graupner, H. Wang, H.W. Gibson, and R.M. Davis. "Characterization of Polymer Light-Emitting Diodes Fabricated by Ionically Self-Assembled Monolayer Technique." Mater. Res. Soc. Proc. v598, BB11.50.1-6, 2000.

Of particular interest to this project are clay / polymer films made using ISAM. [15-18] The initial stages of the research done for this thesis was based on work done by Kleinfeld and Ferguson. Kleinfeld and Ferguson used relatively high solution concentrations of clay (0.2 w%) and polymer (≥ 5.0 w%) to produce clay / polymer films. The deposition time that Kleinfeld and Ferguson used was five seconds, at least one order of magnitude faster than work done in most ISAM studies.

2. Montmorillonite

Montmorillonite is an aluminosilicate clay similar to muscovite (mica) with a typical composition of $Na_xMg_xAl_{2-x}Si_4O_{10}(OH)_2$. Montmorillonite was initially chosen to form the negatively charged layer of the proposed ISAM film. The montmorillonite structure is made of silicate sheets each 1 nm thick with lateral dimensions one or less micron across. The individual sheets are bound together by relatively weak attractions. In aqueous solution, water molecules diffuse in

---

[12] K.M. Lenahan, Y. Wang, Y. Liu, R.O. Claus, J.R. Heflin, D. Marciu, and C. Figura. "Novel Polymer Dyes for Nonlinear Optical Applications Using Ionic Self-Assembled Monolayer Technology." Adv. Mater. v10, p853, 1998.

[13] C. Brands, T. Piok, P. J. Neyman, A. Erlacher, C. Soman, M. A. Murray, R. Schroeder, J. R. Heflin, W. Graupner, D. Marciu, A. Drake, M. B. Miller, H. Wang, H. Gibson, H. C. Dorn, G. Leising, M. Guzy, R.M. Davis. "Photovoltaic Responses In Ionically Self-Assembled Nanostructures Containing Conjugated Polymers And Fullerenes." SPIE Proc. v3937, p51, 2000.

[14] J.R. Heflin, C. Figura, D. Marciu, Y. Liu, and R.O. Claus. "Thickness dependence of second-harmonic generation in thin films fabricated from ionically self-assembled monolayers." Applied Physics Letters. v74, n4, p496, Jan 25, 1999.

[15] Kleinfeld, Elain E. and Ferguson, Gregory S. "Stepwise Formation of Multilayered Nanostructral Films from Macromoleculat Precursors." Science. v265, p370, July 15, 1994.

[16] Lvov, Yuri; Katshiko, Ariga; Izumi, Ichinose; Kunitake, Toyoki. "Formation of Ultrathin Multilayer and Hydrated Gel from Montmorillionite and Linear Polycations." Langmuir. v12, n12, p3038, 1996.

[17] Kotov, N. A; Magonov, S; Tropsha, E. "Layer-by-Layer Self Assembly of Alumosilicate-Polyelectrolyte Composites: Mechanism of Deposition, Crack Resistance, and Perspectives for Novel Membrane Materials." Chemistry of Materials. v10, n3, p886, 1998.

[18] Kotov, N. A. et al. "Mechanism of and Defect Formation in the Self-Assembly of Polymeric Polycation-Montmorillonite Ultrathin Films." Journal of the American Chemical Society. v119, n29, p6821, 1997.

between the sheets, expanding the structure. Once hydrated, individual montmorillonite sheets can be sheared apart from one another under high shear stresses. Single crystal montmorillonite sheets are generally irregular rectangles with dimensions that are given in Figure 2.2. The lateral dimensions of montmorillonite sheets vary from crystal to crystal, however all montmorillonite sheets are 1 nm thick.

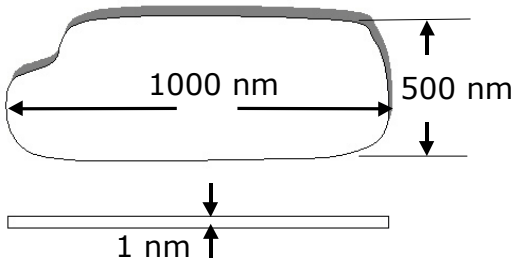

Figure 2.2: A single montmorillonite crystal. [19]

Muscovite has a reported elastic modulus of 200 ± 30 GPa, a K_{IC} of 1.3 MPa $m^{1/2}$ and a Poisson's ratio of 0.24 parallel to its basal plane.[20-22] By virtue of its size and dimensions each montmorillonite sheet will be defect free. From first principles the calculated shear strength of a perfect crystal is given in Equation 2.1.[23] By definition, Equation 2.2 and Equation 2.3 are true and can be substituted into Equation 2.1 to form Equation 2.4.

[19] www.nanoclay.com/s/cornell.html

[20] Piggot, Michael R. Load Bearing Fibre Composites. Peragmon Press. 1980.

[21] Lawn, Brian. Fracture of Brittle Solids 2nd ed. Cambridge University Press. 1993.

[22] Software: Cambridge Engineering Selector, v3. Grant Design Limited Inc.

[23] Hertzberg, Richard W. Deformation and Fracture Mechanics of Engineering Materials, 4th ed. John Wiley & Sons, Inc. 1996.

Equation 2.1: $$\tau_{theo} \approx \frac{G}{2\pi}$$

Equation 2.2: $$G = \frac{E}{2(1+\upsilon)}$$

Equation 2.3: $$\tau = \frac{\sigma}{2}$$

Equation 2.4: $$\sigma \approx \frac{E}{2\pi(1+\upsilon)}$$

τ_{theo}	Theoretical shear strength of a defect free crystal	υ	Poisson's ratio
G	Shear modulus	τ	Shear stress
E	Elastic modulus	σ	Normal stress

Using muskovite's mechanical properties as a substitute for montmorillonite's unreported mechanical properties, each montmorillonite sheet should have a fracture strength of approximately 26 GPa. Although the longitudinal modulus and estimated strength of montmorillonite crystals may be significant, montmorillonite crystals can bend significantly due to their large aspect ratios. Figure 2.3 shows an SEM image of montmorillonite sheets clearly bending while suspended in a gel.[16]

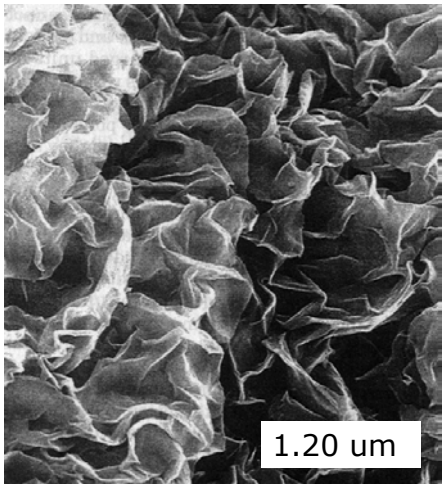

Figure 2.3: SEM image of Montmorillonite sheets bending in a gel.

3. PDDA

Poly(diallyldimethylammonium) chloride (PDDA) is a water soluble poly-cation that was initially chosen for the positively charged layer of the proposed ISAM film. PDDA is always cationic, regardless of pH. PDDA is non-toxic (although skin contact should be avoided, as it may cause irritation) and is used in paper manufacturing. The glass transition temperature of dry PDDA is not recorded in the literature. PDDA is commercially available only in an aqueous solution. The repeat unit of PDDA is given in

Figure 2.4.

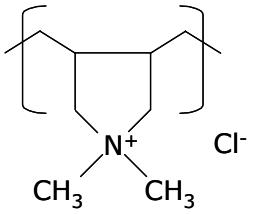

Figure 2.4: The repeat unit of PDDA

4. Description of Nacre

Nacre is the naturally occurring microstructure found in mollusk shells; it is 95 ≥ vol% $CaCO_3$ and 5% organic proteins. Nacre exhibits a 3000 fold increase in work to fracture, and an average fracture toughness 20 times greater than its primary ceramic phase. Mollusk shells have been the subject of interest in materials science and biology due to their surprisingly high strength and fracture toughness.[24-33] The unusually high toughness of nacre is attributed to its unique

[24] Nicholson, Patrick S. "Nature's Ceramic Laminates as Models for Strong, Tough Ceramics." Canadian Ceramics Quarterly. v64, n1, p25, Feb 1995.

[25] Curry, J.D. "Mechanical Properties of Mollusc Shell." Proceedings of the Royal Society of London, Series B. v196, p75, 1977.

[26] Curry, J.D. "Shell Form and Strength," The Mollusca, Vol 11: Form and Function. Academic Press Inc. 1988.

"brick and mortar" microstructure. Nacre is made of flat aragonite platelets arranged in a staggered manner (aragonite is a polymorph of $CaCO_3$). A thin, 20 nm organic matrix surrounds each platelet. Figure 2.5 shows a micrograph of nacre.[29]

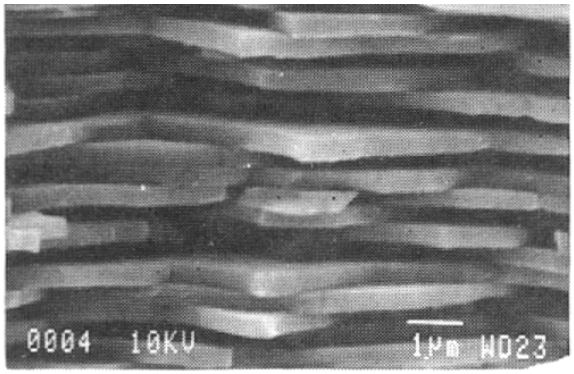

Figure 2.5: SEM micrograph of nacre.

When a crack propagates through nacre, the crack is forced to cut through the relatively weak organic matrix, rather than the $CaCO_3$ platelets. The torturous crack path increases the work of fracture. The matrix is ductile, tough, and exhibits crazing. Figure 2.6 shows fractographs of nacre.[27]

---

[27] A.P Jackson et al. "The mechanical design of nacre." Proceedings of the Royal Society of London, Series B. v234, p415, 1988.

[28] A.P. Jackson and J.F.Vincent. "A Physical Model of Nacre." Composites Science and Technology. v36, n3, p255, 1989.

[29] Morse, Daniel E. et al. Materials Research Society Symposium Proceedings. v292, p59, 1993.

[30] Mehmet Sarikaya and Ilhan A. Aksay. "Synthetic and Biological Nanocomposites." Chemical Processing of Advanced Materials. John Wiley and Sons Inc. 1992.

[31] M. Sarikaya; K.E. Gunnison; M. Yasrebi; I. A. Aksay. "Mechanical Property-Microstructural Relationships in Abalone Shell." Materials Research Society Symposium Proceedings. v174, p109, 1990.

[32] W. J. Clegg. "The Fabrication and Failure of Laminar Ceramic Composites." Acta metallurgica et materialia. vol 40, n11, p3085, 1992.

[33] Bettye L. Smith. "Molecular Mechanistic Origin of the Toughness of Natural Adhesives, Fibres and Composites." Nature. v399, n24, June 1999.

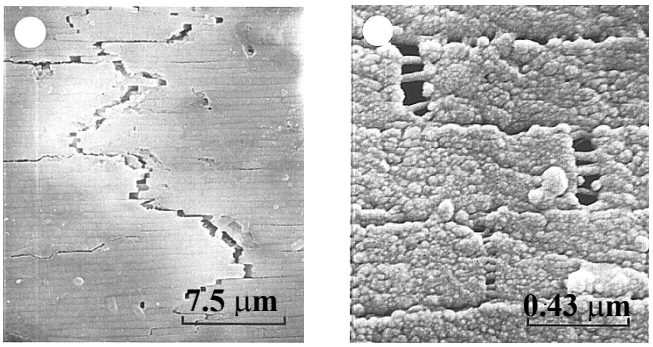

Figure 2.6: SEM images of crack propagation through nacre.

5. Atomic Force Microscopy (AFM)

An atomic force microscope (AFM) will be used to examine the surface of the nanolaminate in intermittent-contact tapping mode. The AFM will show variations in height, elasticity, viscoelasticity, adhesion, and chemical interactions on the sample's surface. Tapping mode AFM works on the following principles: A silicon nitride cantilever with a sharp tip at its end is vibrated at its resonant frequency, between 100 – 400 kHz. On the down stroke of the cantilever, the AFM tip contacts the surface of the sample. A laser beam is deflected off the cantilever into a photodetector; which monitors the cantilever's oscillation. The motion of the laser beam across the photodetector is then translated in a set of instructions for the piezoelectric scanner beneath the sample, which moves vertically to give the cantilever's oscillation a constant amplitude. The vertical adjustments made by the piezoelectric scanner are outputted to a computer and recorded as height variations along the sample's surface. Differences in elasticity, friction, and adhesion on the sample can be measured by the phase mismatch between the cantilever's drive signal and the cantilever's actual oscillation.[34] In the schematic shown in Figure 2.7, the signal driving the oscillation of the cantilever is shown in dashed blue lines, while the actual motion of the cantilever, is a solid red line. Using phase imaging, compliant regions on the sample's surface will contrast against stiffer areas, even if both areas have matching topography. The stack of piezoelectric material beneath the sample controls the

sample's horizontal motion.[34] A schematic of an AFM working in tapping mode is given in Figure 2.7.

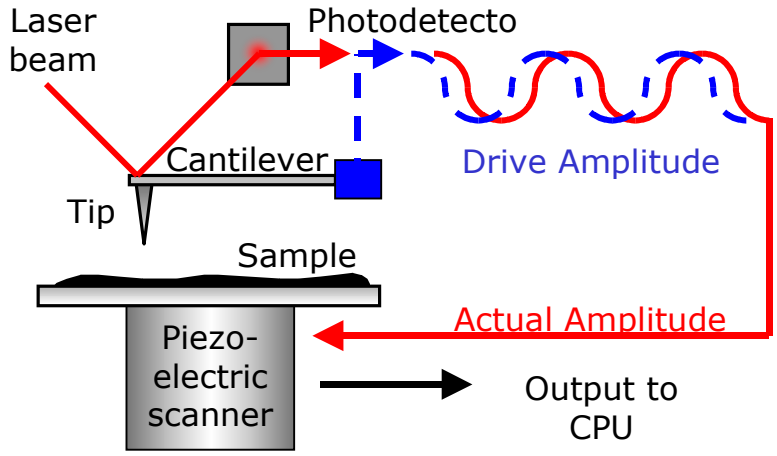

Figure 2.7: A schematic of an AFM running in intermittent-contact tapping mode.

6. Project Summary

The goal of this project is form a thin film with a nacre-like microstructure using ISAM technology. A nacreous nanolaminate may possess excellent mechanical properties for applications as a hard, protective coating. The lamina of the composite will have layer thicknesses ~1 nm or less and will substitute montmorillonite clay sheets and PDDA for the inorganic and organic phases in nacre, respectively. Figure 2.8 gives a schematic of the proposed composite.

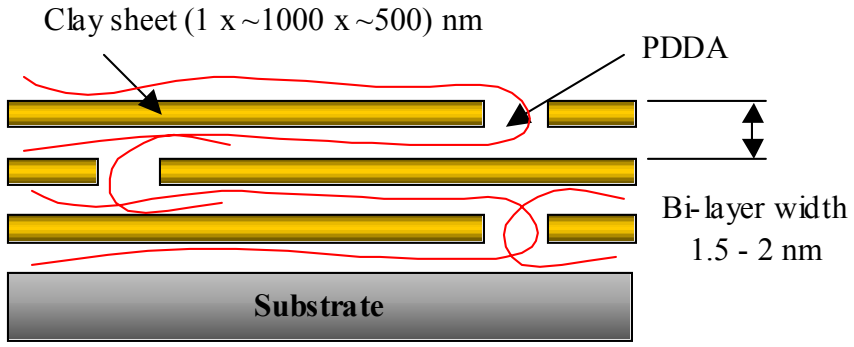

Figure 2.8: Schematic of the proposed montmorillonite / PDDA composite

[34] Howland, Rebecca and Benatar, Lisa. "A Practical Guide to Scanning Probe Microscopy." Informational Pamphlet. Park Scientific Instruments. 1997.

The sheets of montmorillonite will not be deposited in an ordered arrangement, as in nacre, where the center of each sheet is directly above the gap between sheets beneath.

B. Procedure

1. Container Preparation

It is vitally important that glassware and tools used in ISAM processing are kept clean and that containers holding cation or anion solutions are kept separate from each other. In preparation for the processing of the ISAM films, all of the glassware, dipping containers, and other lab equipment that would come in contact with the montmorillonite or PDDA solutions were prepared according to the cleaning procedures listed in the Appendix. Deionized water was provided by a D6311 ROpure ST Reverse Osmosis / Tank System run in series with a Barnstead E-pure system that produced 18 MΩ deionized water. Once deionized, the water was stored in a 100L Nalgene reservoir for use. Half of the cleaned glassware, plastic containers, and one wash tub was labeled "P" and set aside for the exclusive use of mixing and containing PDDA solutions. Likewise, the remaining glassware, containers and wash tub were marked "M" for exclusive use with montmorillonite solutions. Glassware and containers were dried upside down on plastic drying racks; the drying racks had been cleaned with nylon brushes and Sparkleen®, similar to the other lab equipment, and were labeled and devoted to either montmorillonite or PDDA solutions.

2. Solution Mixing

Immediately prior to their use, each 150 mL beaker, which contained a 1 inch Teflon coated stir bar, was rinsed once with deionized water to remove any contaminants that may have accumulated during the beaker's drying. PDDA was purchased from Aldrich Inc. in three different molecular weights, (M_w = 100 –

200 $kg.mol^{-1}$), (200 – 350 $kg.mol^{-1}$), and (400 – 500 $kg.mol^{-1}$). The three molecular weights of PDDA appear throughout this report as LPDDA, MPDDA, and HPDDA, respectively. Solutions of sodium montmorillonite were generously provided by Southern Clay Products (SCP) and Nanocor Inc. Closite® is the trade name of the montmorillonite solution provided by Southern Clay; the montmorillonite solution from Nanocor Inc. had no trade name and is abbreviated Mont throughout this thesis.

Solutions of (PDDA / deionized water) and (clay / deionized water) were mixed in the 150 mL beakers. The top of each beaker was sealed with Parafilm M®. Using a magnetic stirplate, one inch Teflon® stir bars in the beakers were used to stir each solution for a minimum of 18 hours. After each solution was stirred, approximately 100mL of every solution was poured into a staining jar. Each staining jar contained a 0.5" Teflon® coated stir bar; both the jars and the 0.5" stir bars were rinsed with deionized water before use. Every jar was labeled and sealed. Parafilm M® was used to reseal the beakers containing excess solution; each beaker was then set aside for future pH measurements.

3. PH Measurments

Since the effects of pH on solutions of PDDA and montmorillonite are not precisely known, the pH of each solution was measured to ensure reproducibility of the experiment. 30 ± 2 mL of each ISAM solution were poured into 50 mL plastic beakers. An Accumet ® AR15 pH meter was used to measure the pH of each solution; the pH reported by the Accumet ® was allowed to equilibrate for 15 minutes before the solutions' pHs were recorded.

4. Standard ISAM processing

Before a solution was used for ISAM processing, the staining jar holding the ISAM solution, was placed on the lab countertop for use; the jar's top was loosened and then the staining jar was allowed to sit stationary for at least 10 minutes. The 10-minute waiting period gave time for any aggregates that were

disturbed by moving the jar time to settle. Then a pair of metal tweezers was inserted into a mica slide, edge on, and used to cleave a fresh surface off the mica. Both sides of a mica slide were cleaved sequentially, in order to produce a clean and atomically flat surface. One edge of the mica slide was gripped with a plastic pair of Nalgene scissor-type forceps. The cleaved mica slide was then partially inserted into a PDDA solution for a specified time. Ideally, the forceps holding the mica slide did not contact the solution, although they sometimes did for a brief moment. After being dipped into the PDDA solution, the substrate and the ends of the forceps were submerged into a 400 mL beaker filled with ~ 300 mL of deionized water. The beaker was labeled "DP" (for dipping after PDDA). The mica slide was gently moved about in the deionized water for approximately 20 seconds. Afterward the deionized water in the "DP" beaker was poured out over both sides of the mica slide, which was then immersed beneath a flow of running deionized water for approximately 5 seconds. The mica slide was then dried using a jet of N_2 gas. A second, pre-cleaned pair of forceps was used to grip the opposite side of the mica slide and the first pair of forceps was released from the mica slide. The entire process was then repeated using a solution containing montmorillonite rather than PDDA. A 400 mL beaker labeled "DM" (for dipping after montmorillonite) replaced the beaker labeled "DP" during this cycle.

5. Ultrasonic Cleaning

The normal cleaning phase for a number of the ISAM samples was modified with ultrasonic agitation. The cleaning beakers, filled with ~ 300 mL of deionized water, were placed into the Branson 55/0 ultrasonic cleaner and ultrasonically agitated. After polymer or clay deposition was complete, the sample, held with a pair of plastic forceps, was completely submerged into the cleaning beaker while the ultrasonic cleaner was running. The sample was gently moved around the beaker for the prescribed time. Once the cleaning was complete the sample was removed from the cleaning beaker and was dried using a jet of N_2 gas.

6. Agitated Solutions

Some ISAM samples were made using solutions of montmorillonite that had been agitated prior to their use. The preparation of these samples was identical to other samples with the following exceptions. The staining jar filled with the montmorillonite solution was placed into a Branson 55/0 ultrasonic cleaner and agitated for 1 hour prior to use in ISAM deposition. One film was prepared using this montmorillonite solution, cleaning was done following standard ISAM procedures. A second film was prepared using the agitated montmorillonite solution also, but was cleaned using ultrasound. A third film was prepared with the agitated solution, but during the montmorillonite deposition, the staining jar holding the montmorillonite solution was placed in the ultrasonic cleaner while the ultrasound was agitating the solution. The sample was then cleaned with following standard ISAM procedures. A series of clay solutions were exposed to low frequency agitation. Rather than letting the staining jar remain stationary before use, some of the clay solutions were stirred at a speed setting of 2 on a scale of 1 –10 for 5 minutes or shaken by hand.

7. Settled Solutions

Four 25 mL graduated cylinders were cleaned using standard cleaning procedures and then taped down to prevent their motion. Approximately 25 mL of a 2.00 w% montmorillonite solution was deposited in each of the graduated cylinders. The graduated cylinders were then covered with Parafilm M® for 10 days. After the solutions had been allowed to settle for 10 days the top 10 ± 1 mL of each solution was removed by pipette and discarded. The remaining 15 mL of solution in each graduated cylinder was then poured into a 150 mL beaker, covered with Parafilm M® and stirred according to standard ISAM processing.

This solution was prepared after consulting Dr. Giannelis at Cornell.[35] The objective of this procedure was to remove smaller clay sheets from the solution.

8. Sample Mounting and Viewing

Once deposition was complete, a 1 x 1 cm section of mica was cut from the middle of the mica slide and held with a pair of tweezers. An adhesive sticker was used to place adhesive upon an AFM stage piece and the mica adhered to the stage piece. The edges of the mica section were pressed firmly against the stage piece with a pair of tweezers to ensure good adhesion. The stage piece, with the mica section on it, was placed on a strip of magnetic tape. The tape was fastened to the inside of a polystyrene sample holder. The samples were then transported from Luna Innovations's thin film lab to the AFM lab at Virginia Tech. Once loaded onto an AFM stage, the mica sample was viewed using a Nanoscope III scanning tunneling microscope (STM) set on tapping mode.

9. Measurements of PDDA's Tg

An unrecorded amount of 20.00 w% aqueous solution of high molecular weight PDDA (HPDDA) was placed into a 500 mL round bottomed flask. The flask was connected to an in-line vacuum and a 1.5 inch stir bar was placed into the flask and allowed to stir. Once the solution had reached a viscosity high enough that the stir bar could no longer turn, the bottom of the flask was lowered into an evaporating dish half filled with water. The water was heated to a boil, but was never allowed to completely evaporate away, aiding the evaporation process. Once no more water could be evaporated from the nearly solid solution of HPDDA, the solution was placed into a vacuum of 30 μm Hg. Solid pieces of HPDDA were formed from the solutions. The solid pieces of HPDDA were a translucent, nearly opaque, pale yellow. A sample of the solid HPDDA was run

[35] Private communication with Professor E Giannelis, Materials Science and Engineering, Cornell.

inside a thermogravimetric analyzer (TGA) to measure a burn-out temperature in air. Three runs of a dynamic scanning calorimeter (DSC) were used to measure the glass transition temperature from another dried piece of HPDDA.

C. Results

1. Nomenclature

Both height and phase images (see Introduction) of ISAM films were taken using an AFM in tapping mode. In the example image shown in Figure 2.9, an AFM height image is shown on the left, while a phase image of the sample is given on the right. Throughout this thesis, usually only one of either the phase or the height images is given. Often, the phase image offered no additional information and was excluded from the thesis and replaced with a height scale.

The caption of each figure in the results section describes how the sample was processed. Since several parameters were varied a simple code was created to simplify the captions. Below, in Figure 2.9 is a sample caption that is explained in the following paragraph.

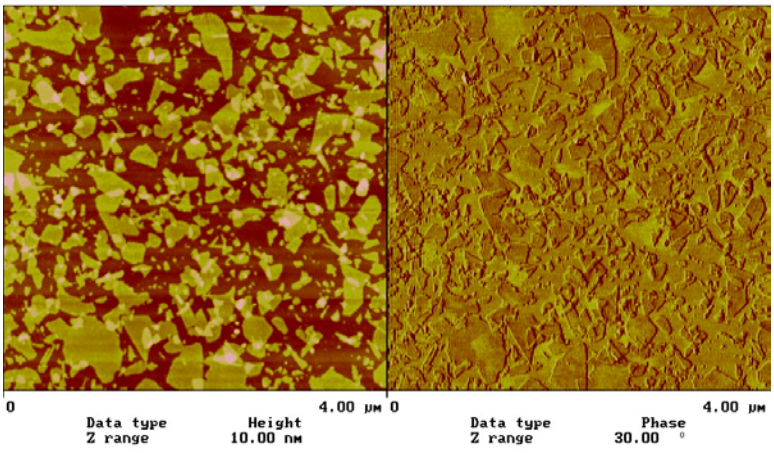

Figure 2.9: An example of an AFM height image (left) and AFM phase image (right) of an ISAM produced thin film on a mica substrate.

((0.02 w% LPDDA, 10 s [Norm]) (0.02 w% Closite® 10 s [10 s US]))$_{1.5}$

Everything about a sample's dip in a solution is described inside a pair of parentheses (). The order of the dips follows from left to right. In Figure 2.9 for example, the substrate was dipped first into a solution of 0.02 w% LPDDA (low molecular weight PDDA) for 10 seconds, followed by a 10 second dip into a solution of Closite® and finished with another dip into a 0.02 w% LPDDA (low molecular weight PDDA) for 10 seconds The subscripted number shows the number of times the whole deposition cycle was carried out, in the above case, polymer, clay, and finally polymer were deposited on the mica substrate. A sample's cleaning procedure after a deposition dip is in brackets []. The example sample shown in Figure 2.9 was cleaned using normal cleaning procedures after dipping in solutions of PDDA and cleaned using ultrasonic agitation for 10 seconds after being dipped in a Closite® solution.

2. Bare Mica and Polymer Covered Mica

Figure 2.10 shows an AFM height image of a freshly cleaved substrate of mica. Both the average and root mean squared roughness of the mica substrate were < 2 angstroms. Circular height aberrations were common on cleaved mica surfaces, their presence may be caused by defects in the mica itself, or a contaminant from the environment. Height ridges on the mica are the result of the mica bowing.

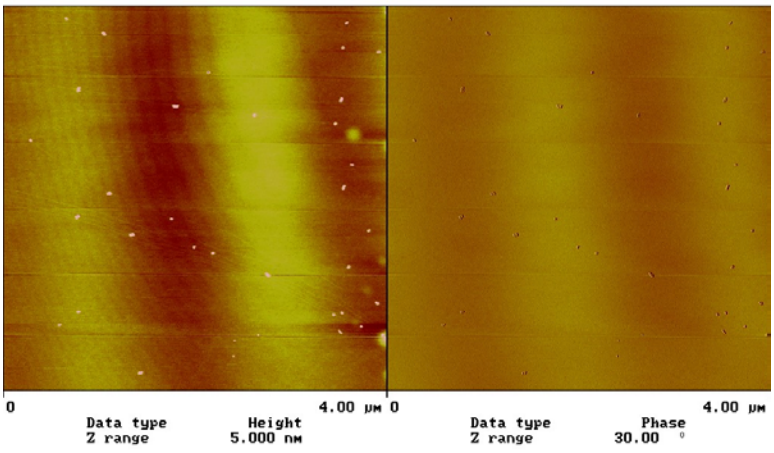

Figure 2.10: AFM height image (left) and phase image (right) of a cleaved mica substrate.

A mica substrate covered with polymer is given in Figure 2.11. The polymer layer, although present, is unnoticeable.

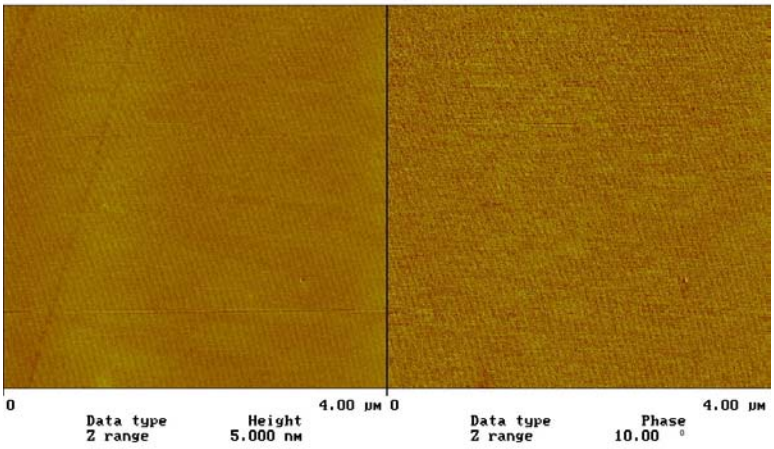

Figure 2.11: AFM height image (left) and phase image (right) of an ISAM produced thin film on a mica substrate.

$(0.20\ w\%\ LPDDA,\ 10\ s\ [Norm])_{1.0}$

3. Closite® Terminated ISAM films

Figure 2.12 - Figure 2.15 show fragments of clay sheets deposited during ISAM deposition. The clay sheet fragments are asymmetric with a constant vertical dimension of ~ 1 nm and lateral dimensions varying between 10 – 1000 nm. As the concentration of clay was increased during ISAM deposition, the amount of clay deposited also increased. Individual clay platelets became indistinguishable when a solution of 2.95 w% clay was used during the ISAM process. The clay fragments frequently overlapped one another as can be seen in several of the figures. While overlapping one another the clay platelets conformed to the surface of the clay platelets beneath them.

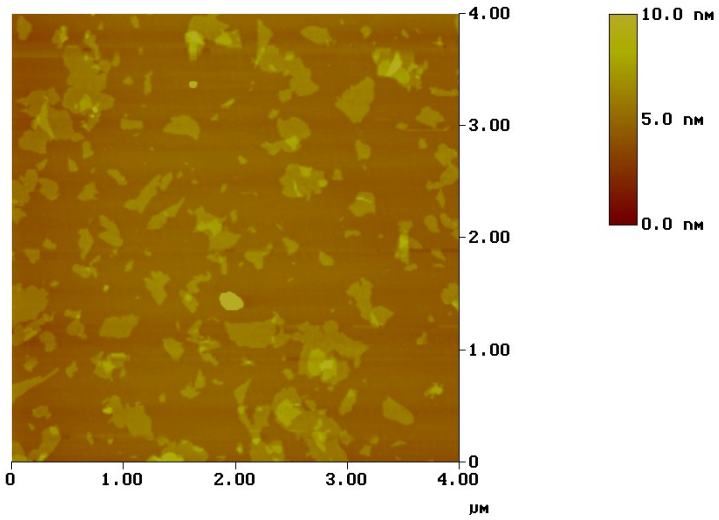

Figure 2.12: AFM height image of an ISAM produced thin film on a mica substrate. ((0.02 w% LPDDA, 10 s [Norm]) (0.02 w% Closite® 10 s [Norm]))$_{1.0}$

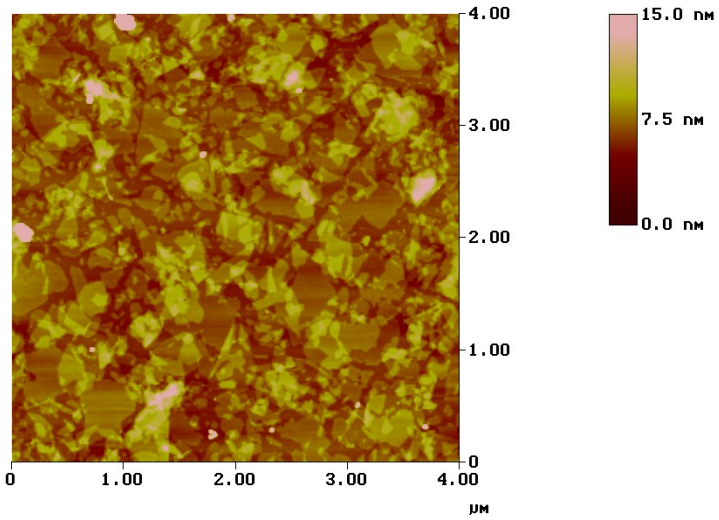

Figure 2.13: AFM height image of an ISAM produced thin film on a mica substrate. ((0.02 w% LPDDA, 10 s [Norm]) (0.20 w% Closite® 10 s [Norm]))$_{1.0}$

Agglomerates of clay, or possibly inorganic contaminants are noticeable in the ISAM sample shown in Figure 2.14. These contaminants have the highest vertical dimensions in the image, but have a circular footprint on the surface; it is likely that these contaminants are spherical.

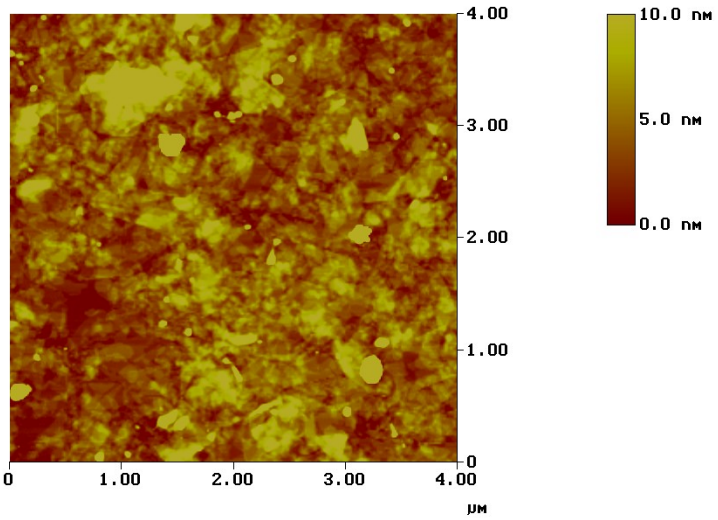

Figure 2.14: AFM height image of an ISAM produced thin film on a mica substrate. ((0.02 w% LPDDA, 10 s [Norm]) (2.95 w% Closite® 10 s [Norm]))$_{1.0}$

Figure 2.15 shows that it is possible to completely cover the surface of the substrate in less than 5 seconds with clay particles.

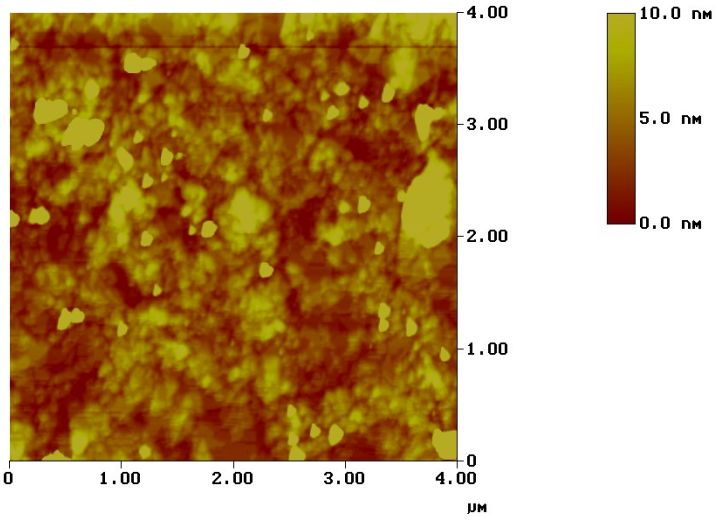

Figure 2.15: AFM height image of an ISAM produced thin film on a mica substrate. ((0.02 w% LPDDA, 5 s [Norm]) (2.95 w% Closite® 5 s [Norm]))$_{1.0}$

Overlapping of the clay platelets is clearly shown in Figure 2.16 though Figure 2.18. When the clay platelets overlap they conform to the surface of the platelet beneath them. The platelets' apparent lack of stiffness is due to their very

large (> 200) aspect ratios. The sample in Figure 2.18 has been sectioned; the section is given in Figure 2.19. The expected height of each clay platelets was ≈ 1 nm, which is what is experimentally observed in Figure 2.19. The 2 nm vertical difference between the a-markers is caused by a 40 x 15 nm clay platelet laying on top of two other clay platelets. There is some height variation along the individual clay platelets on the angstrom level, presumably due to the mica substrate bending, or noise in the data.

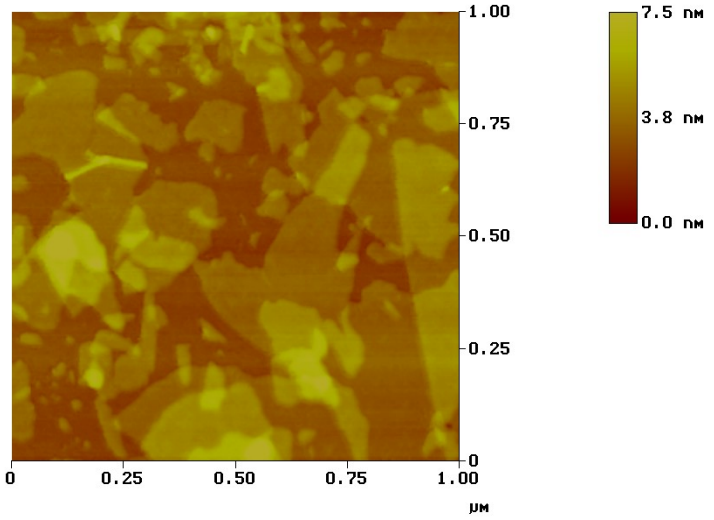

Figure 2.16: AFM height image of an ISAM produced thin film on a mica substrate showing the edges of clay fragments overlapping

((0.02 w% LPDDA, 10 s [Norm]) (0.20 w% Closite® 10 s [Norm]))$_{1.0}$

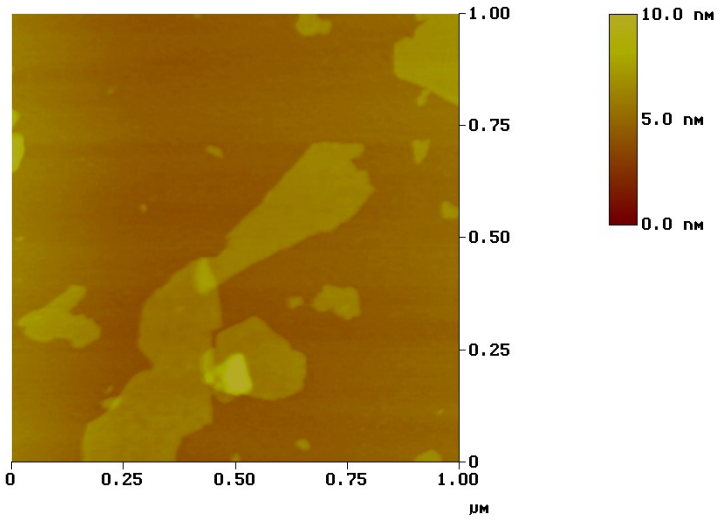

Figure 2.17: AFM height image of an ISAM produced thin film on a mica substrate showing the edges of clay fragments overlapping

((0.02 w% LPDDA, 10 s [Norm])(0.02 w% Closite® 10 s [Norm]))$_{1.0}$

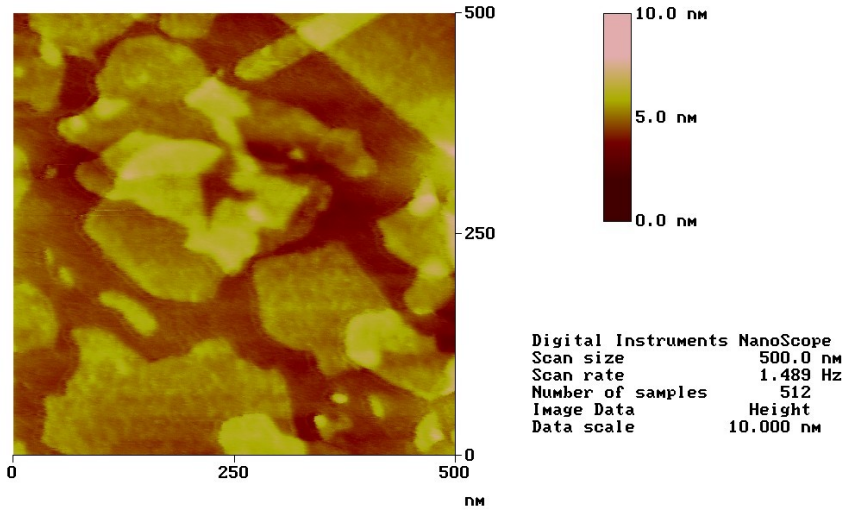

Figure 2.18: AFM height image of an ISAM produced thin film on a mica substrate showing the edges of clay fragments overlapping

((0.02 w% LPDDA, 10 s [Norm]) (0.20 w% Closite® 10 s [Norm]))$_{1.0}$

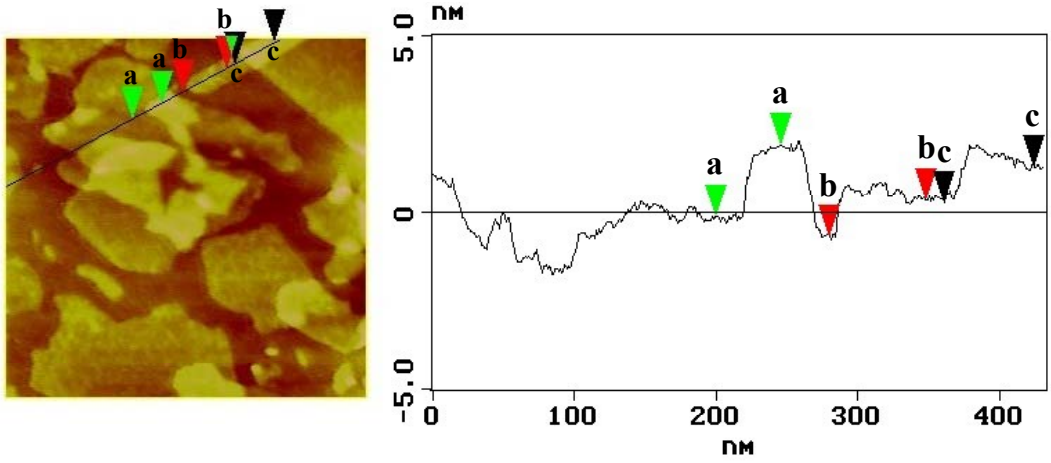

Figure 2.19: A height section of Figure 2.18.

Table 2.1: Height differences between makers on the section of Figure 2.18

Maker pair	Height difference (nm)
a	2.038
b	1.086
c	1.010

4. Montmorillonite Terminated ISAM films

Figure 2.20- Figure 2.23 show samples of the clay / polymer nanocomposite that were produced using PDDA and the montmorillonite that was donated by Nanocor Inc. ISAM films made using a concentration of 0.02 w% Mont show individually distinguishable clay platelets, regardless of the length of deposition time. Once the concentration of the clay solution is increased to 0.20 w% and above, deposition of the clay particles is no longer limited to a single monolayer of clay platelets. Deposition of the clay sheets becomes uncontrolled; clay particles begin adhering to one another rather than repelling each other via electrostatic forces. The uncontrolled deposition of the clay results in significant height variations on the sample's surface where individual sheets of clay are no longer visible.

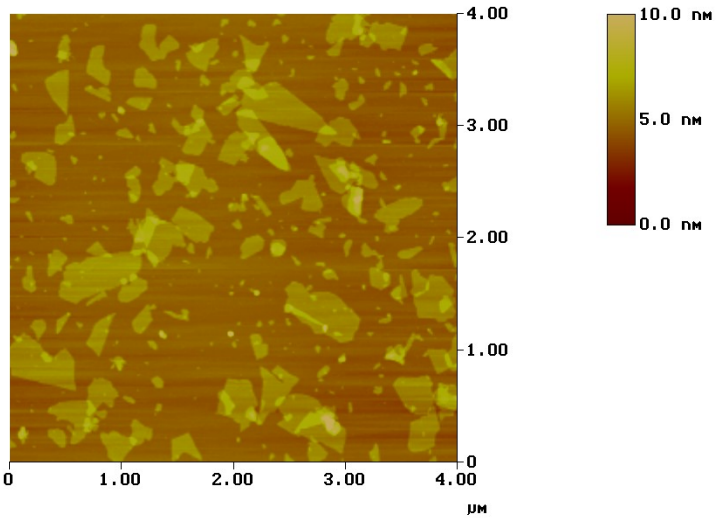

Figure 2.20: AFM height image of an ISAM produced thin film on a mica substrate. ((0.02 w% LPDDA, 10 s [Norm]) (0.02 w% Mont 10 s [Norm]))$_{1.0}$

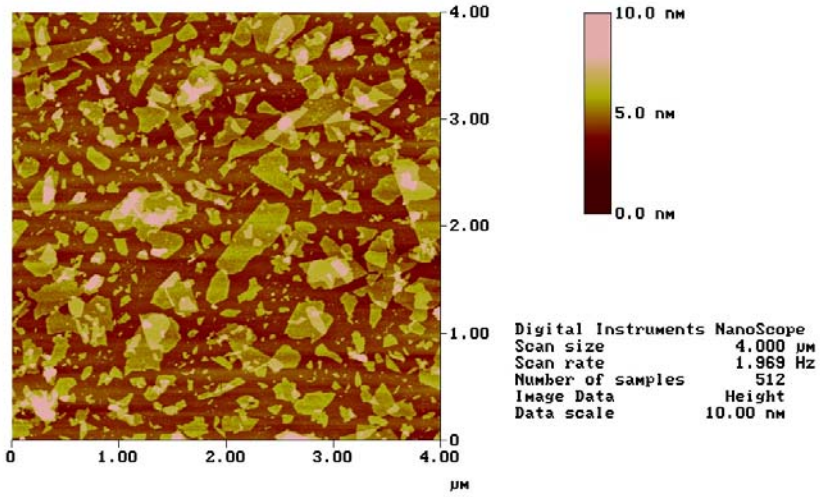

Figure 2.21: AFM height image of an ISAM produced thin film on a mica substrate. ((0.02 w% LPDDA, 10 s [Norm]) (0.02 w% Mont 600 s [Norm]))$_{1.0}$

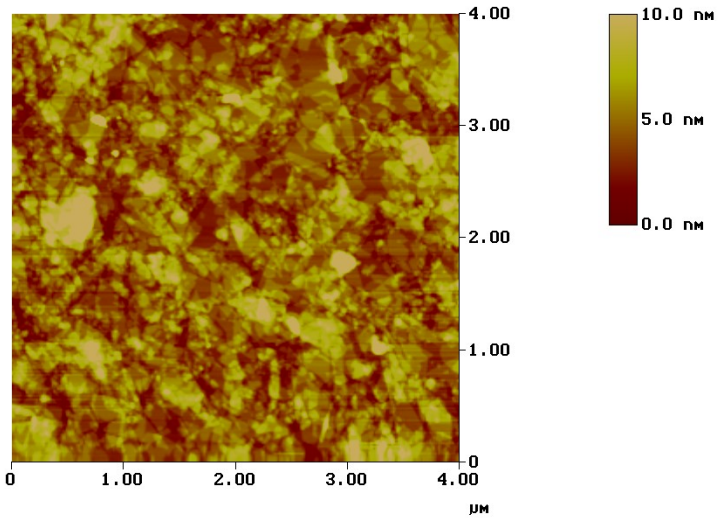

Figure 2.22: AFM height image of an ISAM produced thin film on a mica substrate. ((0.02 w% LPDDA, 10 s [Norm]) (0.20 w% Mont 10 s [Norm]))$_{1.0}$

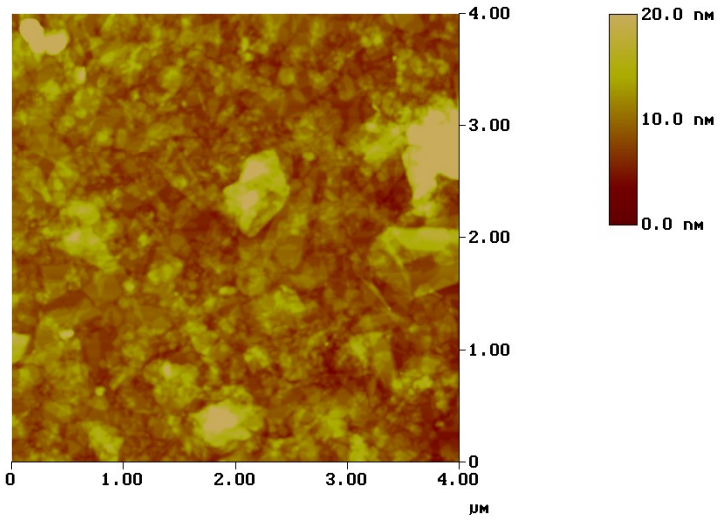

Figure 2.23: AFM height image of an ISAM produced thin film on a mica substrate. ((0.02 w% LPDDA, 10 s [Norm]) (2.00 w% Mont 10 s [Norm]))$_{1.0}$

5. The Effect of Ultrasonic Cleaning

Comparing Figure 2.20-Figure 2.23 to Figure 2.24-Figure 2.26 it is clear that ultrasonic cleaning during the wash phase of ISAM deposition greatly affects the samples' microstructures. The latter set of samples, cleaned using ultrasonics, has a substantially smoother surface; and individual platelets are clearly distinguishable.

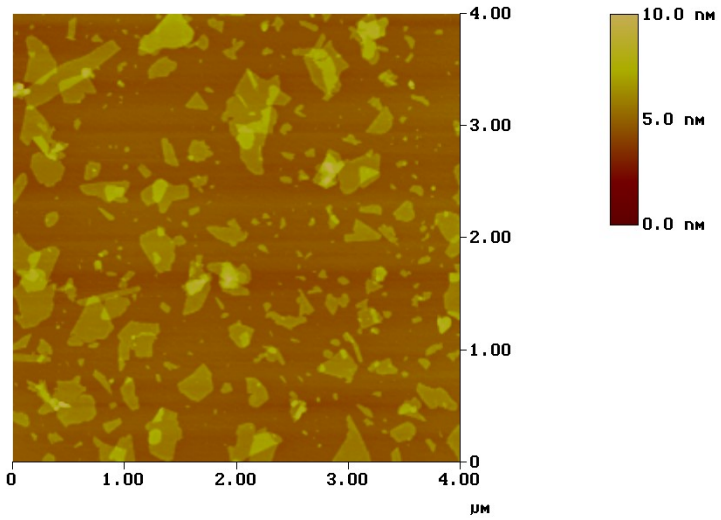

Figure 2.24: AFM height image of an ISAM produced thin film on a mica substrate. ((0.02 w% LPDDA, 10 s [Norm]) (0.02 w% Mont 10 s [US 10 s]))$_{1.0}$

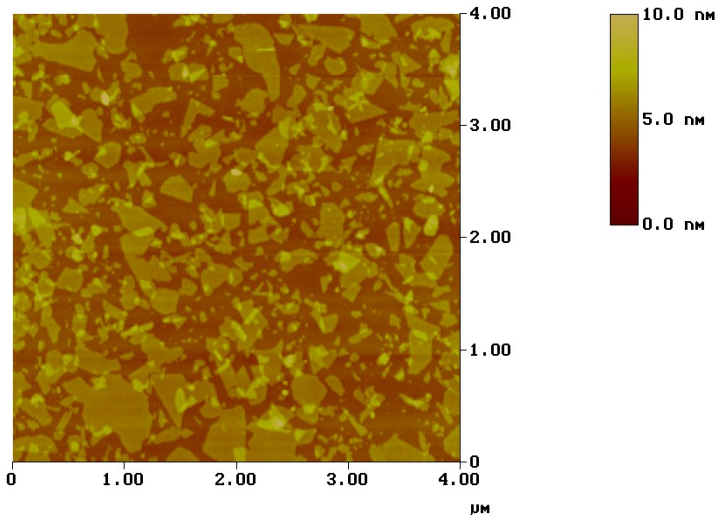

Figure 2.25: AFM height image of an ISAM produced thin film on a mica substrate. ((0.02 w% LPDDA, 10 s [Norm]) (0.20 w% Mont 10 s [US 10 s]))$_{1.0}$

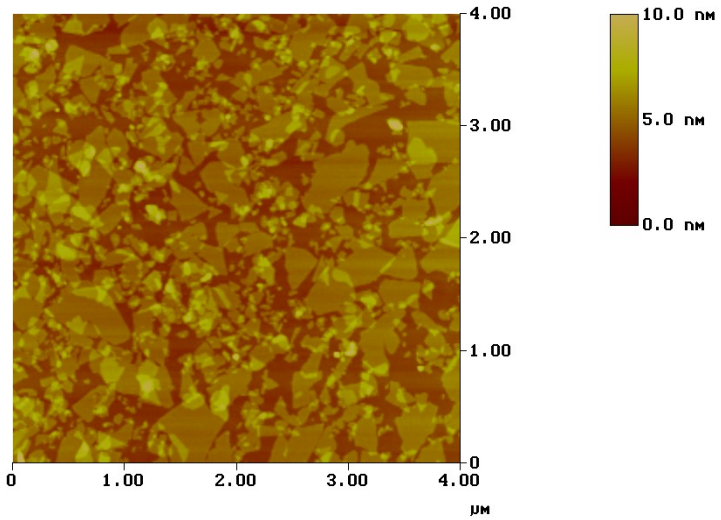

Figure 2.26: AFM height image of an ISAM produced thin film on a mica substrate. ((0.02 w% LPDDA, 10 s [Norm]) (2.00 w% Mont 10 s [US 10 s]))$_{1.0}$

6. Clay Deposition without Polymer Present

Deposition of clay directly upon the mica substrate without a preceding layer of PDDA was severely limited, as seen in Figure 2.27 - Figure 2.29. As the concentration of the clay increased in solution from 0.02 – 2.00 w%, the deposition of the clay also increased on the bare mica substrate, but was very limited compared to substrates covered with PDDA. Raised surfaces on the mica substrate, which appear as blurred lines in Figure 2.27 and Figure 2.28 are either imaging affects caused by the AFM or bowing of the mica substrate.

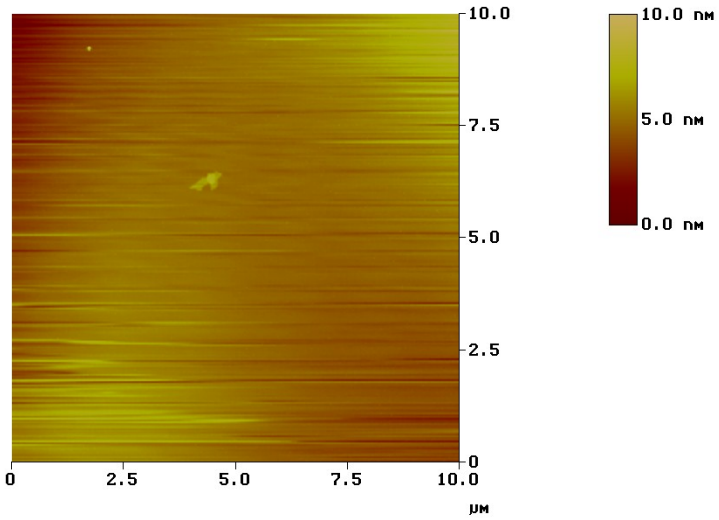

Figure 2.27: AFM height image of an ISAM produced thin film on a mica substrate. (0.02 w% Mont 10 s [Norm])$_{1.0}$

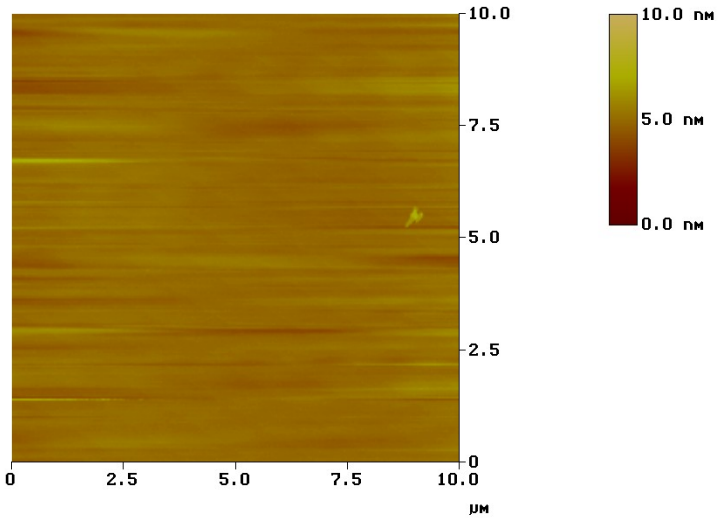

Figure 2.28: AFM height image of an ISAM produced thin film on a mica substrate. (0.20 w% Mont 10 s [Norm])$_{1.0}$

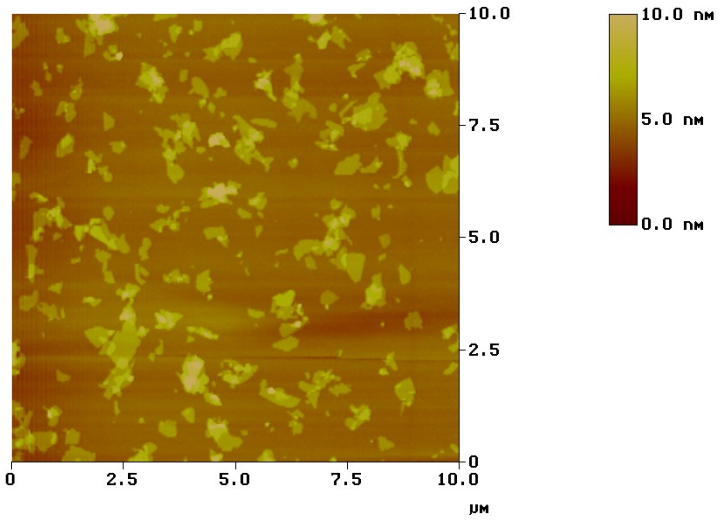

Figure 2.29: AFM height image of an ISAM produced thin film on a mica substrate. (2.00 w% Mont 10 s [Norm])$_{1.0}$

7. Polymer Concentration Effects on Clay Deposition

Higher concentrations of PDDA led to higher depositions of clay for solutions made under similar conditions, which is demonstrated by the microstructures of the samples shown in Figure 2.30 and Figure 2.31.

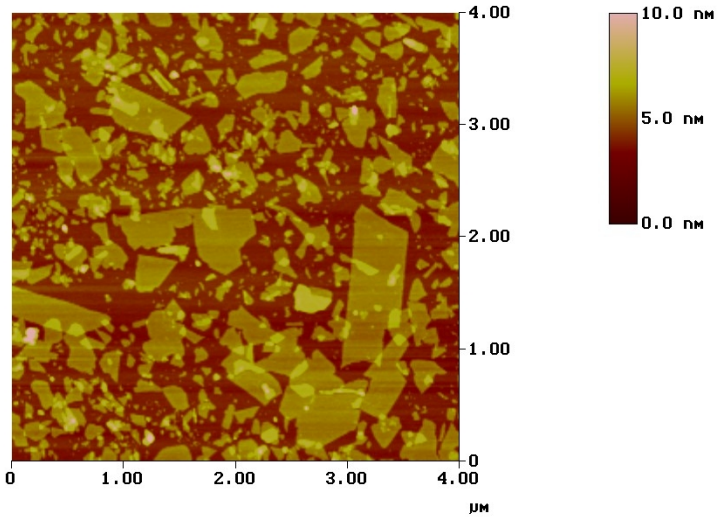

Figure 2.30: AFM height image of an ISAM produced thin film on a mica substrate. (0.02 w% LPDDA, 600 s [US 10 s]) (0.20 w% Mont 10 s [US 10 s])$_{1.5}$

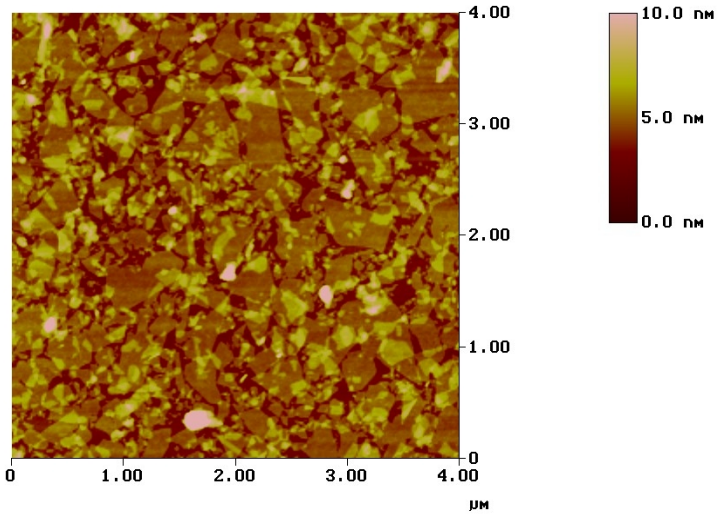

Figure 2.31: AFM height image of an ISAM produced thin film on a mica substrate. (1.00 w% LPDDA, 600 s [Norm]) (0.20 w% Mont 10 s [US 10 s])$_{1.5}$

8. ISAM Films Produced using Agitated and Settled Solutions

The clay solutions used to produce the thin films shown in Figure 2.32 and Figure 2.33 were agitated using ultrasound for an hour before being used in the ISAM process. The pre-agitation of the clay solutions did not affect the microstructure of the resulting ISAM film. The ISAM film shown in Figure 2.33 was formed using the pre-agitated solution and in addition, the container holding the clay solution was exposed to ultrasound while the substrate was put into the clay solution. Using ultrasound during the clay deposition step also did not affect the microstructure of the ISAM film. The ISAM film shown in Figure 2.34 was produced using a settled solution of clay (see Procedure). The microstructure of the film did not show any appreciable difference between a film made from a non-settled solution of clay of the same concentration. Several ISAM films were made using clay solutions that had been agitated at a low frequency (using Teflon® covered stir bars or shaking by hand) before deposition took place. Low frequency agitation of the clay solutions stirred up particles of clay that had previously precipitated out of the clay solutions. The result was that large agglomerates of clay deposited on themselves on the substrate. The surfaces of these samples were difficult and sometimes impossible to image on the AFM.

These images had no distinguishable characteristics and consisted of random height variations on the substrate surface caused by agglomerates of clay.

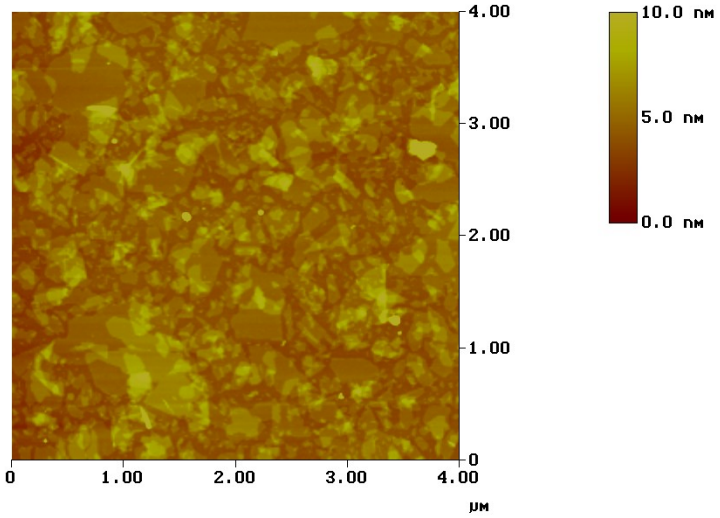

Figure 2.32: AFM height image of an ISAM produced thin film on a mica substrate. The clay was exposed to ultrasonics prior to deposition.

((0.02 w% LPDDA, 10 s [Norm]) (0.20 w% Closite® 10 s [Norm]))$_{1.0}$

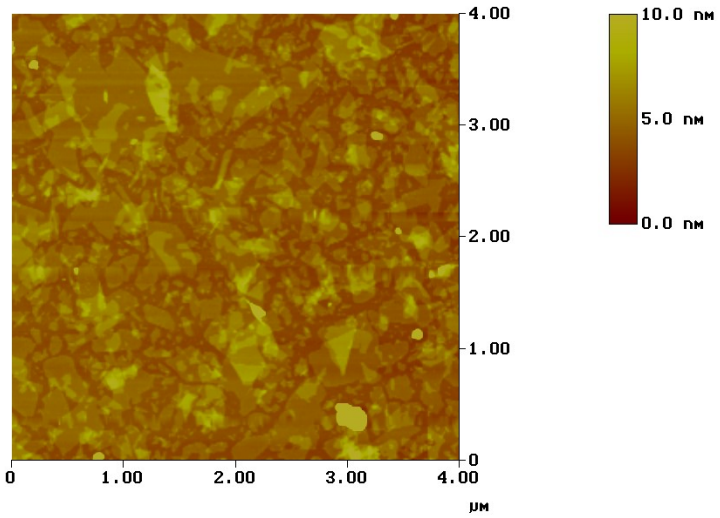

Figure 2.33: AFM image of an ISAM produced thin film on a mica substrate. The clay was exposed to ultrasonics prior to and during deposition.

((0.02 w% LPDDA, 10 s [Norm]) (0.20 w% Closite® 10 s [Norm]))$_{1.0}$

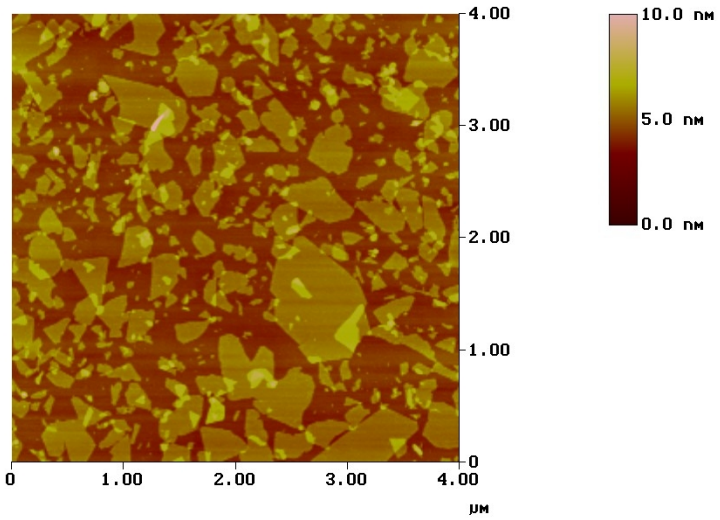

Figure 2.34: AFM image of an ISAM produced thin film on a mica substrate. The clay was allowed to settle in a graduated cylinder before deposition.

((0.02 w% LPDDA, 10 s [US 10 s]) (0.20 w% Mont 10 s [10 s US]))$_{1.0}$

9. Multiple Bi-layer ISAM films

Multiple bi-layer ISAM films were made and imaged using AFM. The mica substrates were found to cleave under the stress of repeated dipping and drying. As a result, AFM images of these samples are highly suspect; there is no way of telling if the mica cleaved during the deposition or not. Images of these samples are not included in this section of the thesis.

10. PHs of ISAM solutions

The pHs of the ISAM solutions varied as a function of concentration. Montmorillonite solutions from both suppliers, SCP and Nanocor were basic and had increasing pHs as their solution concentrations increased. The PDDA solutions were acidic, with increasing acidity as a function of concentration and molecular weight. The measured pHs are given in Table 2.2.

Table 2.2: Solution concentrations of PDDA and Mont with their corresponding pH's

Solution concentration (± 0.02 w%)	pH (± 0.1)
0.02 w% high Mw. PDDA	5.6
0.20 w% high Mw. PDDA	4.4
1.00 w% high Mw. PDDA	3.6
0.02 w% low Mw. PDDA	6.3
0.20 w% low Mw. PDDA	6.0
1.00 w% low Mw. PDDA	5.7
5.00 w% low Mw. PDDA	5.3
10.00 w% low Mw. PDDA	5.5
20.00 w% low Mw. PDDA	5.3
0.02 w% Closite®	7.5
0.20 w% Closite®	7.8
1.00 w% Closite®	8.3
2.95 w% Closite®	8.7
0.02 w% Mont	7.1
0.20 w% Mont	8.8
2.00 w% Mont	10.1

11. Tg of PDDA

The Tg of dried HPDDA was measured to be 231 ± 5 ^{o}C. The degradation temperature of dried HPDDA in air was 275 ± 5 ^{o}C.

D. Discussion

1. Comparison of Clay Solutions

There was a significant difference in viscosity and color of the montmorillonite solutions obtained. The Closite® solution, provided by Southern Clay Products, was a viscous yellowish brown, while the Mont solution, provided by Nanocor Inc. was less viscous and was a dull lavender. Neither clay solution contained any dispersants or additives. Intact stacks of montmorillonite sheets were observed only in the Closite® solution (Unusual Morpholgies and Patterning of ISAM Films).

2. Polymer Creep and Platelet Overlapping

Kleinfield and Ferguson reported deposition of multiple clay layers during an ISAM process for a single dip in a solution of clay.[15] They hypothesized that their deposited polymer layer would "creep" over and cover the surface of clay platelets allowing for the deposition of another clay layer. Figure 2.35 shows a schematic of polymer creep occurring.

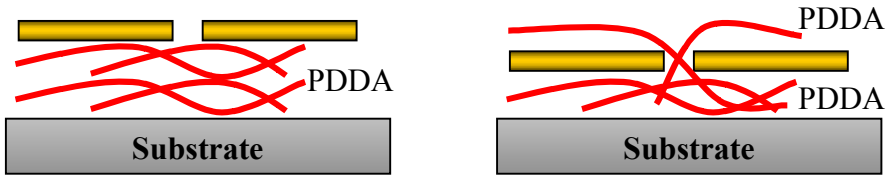

Figure 2.35: Schematic of the polymer "creep" effect.

It is hypothesized that this polymer "creep" effect contributes to the overlapping of the clay platelets. While in an aqueous environment, PDDA chains may be mobile enough and are driven by columbic attraction to climb over at least part of a deposited platelet. Thus, some of a deposited clay platelet assumes the charge of the polymer and accommodates overlapping platelets. Kotov et al also observed platelet overlapping in their work with PDDA and

montmorillonite.[17] Polymer creep is not necessary for overlapping platelets, however. As can be clearly seen at clay concentrations ≥ 0.2 w%.

3. Effects of PDDA Concentration on Deposition

When PDDA was not used to cover the mica substrate, clay deposition was severely limited, but not completely absent. The deposition of a few clay platelets indicates that anionic contaminant probably exist in the clay solutions. Otherwise, the lack of deposition without the presence of PDDA clearly indicates that the ISAM process is functioning as hoped.

Higher concentrations of PDDA, from 0.20 to 1.00 w%, led to increased deposition of clay, as shown in Figure 2.30 and Figure 2.31. Assuming that the PDDA molecules are mobile enough to scale the surfaces of clay platelets, the increased amount of PDDA present allows more of the deposited clay platelets' surfaces to be covered with PDDA. This in turn, supplies more sites for clay platelets to attach themselves to the substrate. At

4. Effects of Clay Concentration on Deposition

Higher clay concentrations resulted in increased clay deposition. Films made with 0.2 w% ≥ solutions of montmorillonite showed uncontrolled deposition of clay. Lvov et al, also observed uncontrolled deposition of montmorillonite in a similar ISAM film when the clay solutions reached 0.1 w%.[16] Further more, both in Lvov's work and in Figure 2.21, samples made with ≤ 0.03 w% montmorillonite solutions showed that the surface of the ISAM films reaches a saturation point where further deposition is inhibited.

Normally, clay sheets align themselves parallel to each other by Van der Waals forces. If solution concentrations of clay exceed some critical amount (≥ 0.03 w%) clay platelets in solution may begin to attract each other and reform into stacks of silicate sheets. Then, when an oppositely charged substrate is made available, a stack of clay platelets, rather than a single platelet attaches itself to the

substrate. Initially deposited platelets are firmly attached to the positively charged PDDA by columbic attraction, while the upper, stacked platelets are attached to the underlying clay by weak Van der Waals forces. Additional clay sheets in solution, driven by long range Van der Waals forces, also deposit themselves on the growing "mound" of clay sheets. Since the additional clay is loosely bound to the substrate, ultrasonic agitation is sufficient to remove the loosely bound platelets that are attached by secondary forces. A cartoon of this is shown in Figure 2.36. Thus, it is practical to use high concentrations of clay to rapidly deposit the clay phase and ultrasonic agitation to create the desired microstructure of a monolayer of clay.

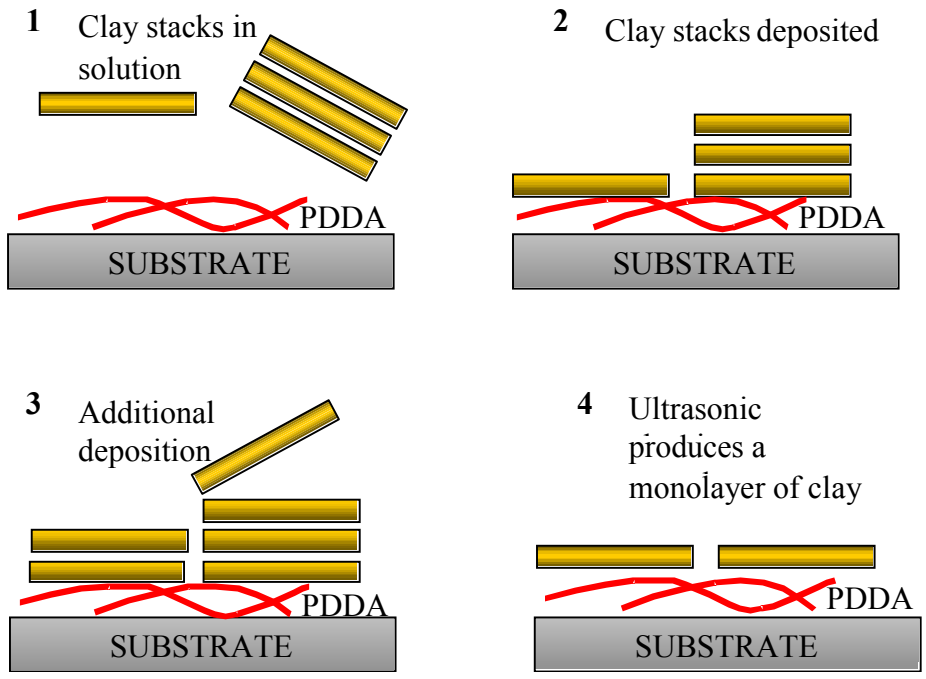

Figure 2.36: Clay deposition and cleaning using a high concentration clay solution

5. Pre-agitated and Settled Solutions

Pre-agitation of the solutions did not produce any desirable results. Low frequency pre-agitation of the solutions by either stir bar or hand forced agglomerates, which had previously dropped out of solution back into solution.

Deposition of these agglomerates onto the substrate made it difficult or impossible to image the ISAM film on the AFM.

It was hoped that the clay solutions that were allowed to settle and were then pipetted would only have large clay platelets present. The ISAM sample made from this solution is shown in Figure 2.34. There are two explanations for why there was no difference in the average size of the clay platelets seen on the sample that used the settled solution. First, ten days was not enough time for the clay to settle in the graduated cylinders. Second, the average size of the clay platelets was actually larger in this solution, but ultrasonic agitation during the cleaning stage fragmented the larger platelets.

Ultrasonic agitation of the clay solutions during clay deposition did not have any effect on the microstructure. Ultrasonic agitation clearly removes loosely bound sheets of montmorillonite, however. Uncontrolled deposition of the platelets may have occurred on the sample shown in Figure 2.33 after the substrate has been removed from the clay solution, but before the sample was placed in the cleaning beaker. This would mean that the amount of residual clay solution present on the substrate after being removed from the solution is quite significant. It is more probable, however, that the concentration gradient between the substrate and the bulk solution had an impact on deposition. Work done by Lvov et al, using PDDA and silica nanoparticles supports the hypothesis that diffusion is a factor in ISAM deposition.[36] As a result, only ultrasonic cleaning in a solution already not saturated with clay removes substantial amounts of clay.

6. Multi-layer films

The failure to make reproducible mutlti-layer films on mica was due to the mica cleaving during deposition. Multi-layer films of PDDA and montmorillonite can be made however, a more suitable substrate is required.[16,17,18]

[36] Lvov et al. "High speed multiplayer film assembly by alternate adsorption of silica." Chemical Communications. v11, p1229, 1998.

E. Conclusion

The ISAM process for a (PDDA / Mont) system was successful. Solution concentrations of clay above 0.02 w% lead to uncontrolled deposition of clay platelets on the substrate's surface. Ultrasonic agitation can be used to remove loosely bound clay platelets and create a desirable microstructure. By using solution concentrations of clay above 0.02 w% and ultrasonic agitation together it is possible to deposit a monolayer of clay platelets on a mica substrate in ≤ 20 seconds.

The PDDA molecules show a high degree of mobility. PDDA molecules beneath clay platelets are capable of "creeping" over the edges of clay platelets and covering the top faces of the platelets if enough polymer is present to do so. This "creep" effect confirms the work done by Kleinfeld and Ferguson.[15] Overlapping of montmorillonite platelets in ISAM films, which is caused by "creeping" of the polymer, was also noticed by Kotov, Magonov and Trophsa.[17]

CHAPTER 3: UNUSUAL MORPHOLOGIES AND PATTERNING OF ISAM FILMS

A. Introduction

1. ISAM Patterning in Literature

To date, patterning using ISAM techniques is essentially a variation upon basic patterning techniques used in the micro fabrication of silicon.[4, 537] Micro-contact printing or photolithography is used in ISAM patterned films to create positively or negatively charged regions upon the substrate. The patterned substrate is then inserted into the desired solution, deposition occurs, and the substrate is cleaned. Figure 3.1 shows a patterned arrangement of gold disks upon a thiol-patterned gold substrate.[37] Patterning and the formation of other unusual morphologies using ISAM films in this work was the result of serendipity.

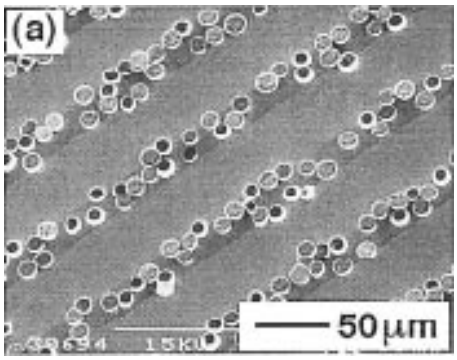

Figure 3.1: A patterned arrangement of ISAM deposited gold disks on a silicon substrate.

2. Laponite

Laponite® is a synthetic magnesium lithium silicate produced by Laporte Industries. When stirred in deionized water, individual platelets of Laponite, each 1 nm thick and 25 nm in diameter, disperse into solution and become negatively

[37] Tien, Joe; Terfort, Andreas; Whitesides, George M. "Microfabrication through Electrostatic Self-Assembly." Langmuir. v13, n20, p5349, 1997.

charged. Several different grades of Laponite® exist. Laponite RD® was used in this study, and will be abbreviated as Laponite throughout the rest of this thesis.

3. Polystyrene Sulfonic Acid Sodium Salt

Polystyrene sulfonic acid sodium salt (PSS), a polyelectrolyte, was purchased from Polysciences Inc. The PSS had a Mw = 70 $kg.mol^{-1}$. PSS is a commonly used polyanion in ISAM literature; its repeat unit is given in Figure 3.2.[3-7]

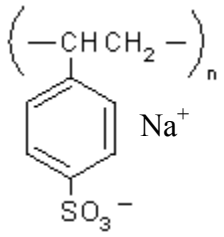

Figure 3.2: Repeat unit of Poly(styrenesulfonate sulfonic acid) sodium salt

B. Procedure

1. Silicon Wafer Preparation

Silicon wafers were obtained from four different vendors for use. Table 3.1 gives the vendor names and the specification of the wafers they provided. All of the wafers were 4 inches in diameter and between 500 – 600 μm thick. The wafers provided by Motorola Inc. were a generous gift from Dr. Hendricks, Virginia Tech.

Table 3.1: Specifications of silicon used and their vendors

Vendor	Dopant	Type	Resistivity (Ω cm)	Face
Wafer World Inc.	Unknown	N	1 – 10	<100>
Virginia Semi-conductor Inc.	Phosphorus	N	5 –10	<100>
MEMC Electronic Materials Inc.	Boron	P	16 – 24	<100>
Motorola Inc.	Boron	P	5 – 22	<100>

Wafers were scribed and cleaved into 1 x 7 cm pieces using a diamond scribe; the pieces were then stored in a polystyrene case with a foam bottom until use. The silicon pieces were cleaned using deionized water in a 5510 Branson Ultrasonic Cleaner for 1 minute. After cleaning, the wafers were dipped into the corresponding ISAM solutions. Silicon assumes a negative surface charge in an aqueous solution of neutral pH due to the attachment of hydroxyl groups. After dipping, the sample was cleaned using either ultrasonic or an improved manual cleaning technique; the improved manual cleaning procedure is outlined in the Appendix. After ISAM film deposition was completed the samples were mounted and viewed using AFM as dictated in the prior Procedure section.

C. Results

1. Bare Silicon

AFM images of the bare silicon substrates showed that the silicon was essentially featureless with an average roughness less than five angstroms. The AFM phase image shown in on the right in Figure 3.3 is unique, in that it shows circular polishing marks or possibly atomic steps on the surface of the substrate.

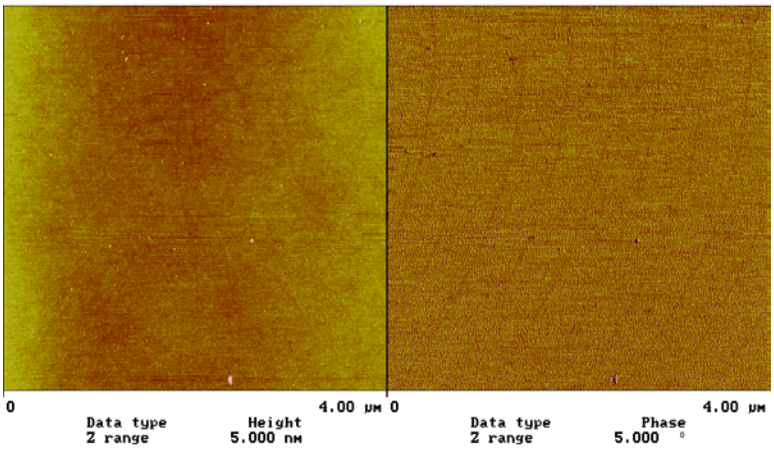

Figure 3.3: AFM height (left) and phase (right) images of silicon from MEMC.

2. Sample Nomenclature

Many of the samples shown in this section of the thesis were made with a sequence of polymer or clay deposition steps that would be cumbersome to list below each figure. To improve readability, the deposition sequence used to make the morphologies shown in this section will be given in the Appendix.

3. Unusual Polymer Morphologies

PDDA assumed a number of unusual morphologies, all of which occurred when relatively high, > 4 w%, concentrations of PDDA were used. One such morphology is the "maze" morphology, shown in Figure 3.4. The maze morphology is characterized by PDDA forming a branching network of linear patterns on the substrate. The thickness of the patterns and the degree of branching varied between mazes on different substrates. Mazes were formed with concentrations of 3 w% ≥ HPDDA and 5 w% ≥ LPDDA.

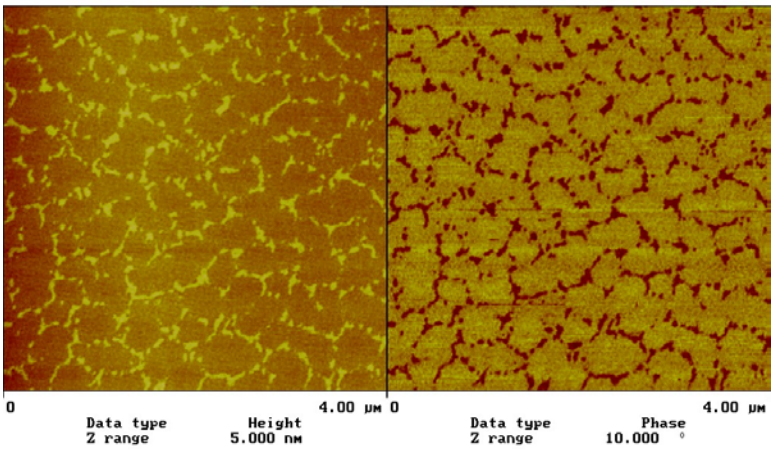

Figure 3.4: AFM height (left) and phase (right) images of a PDDA maze morphology on mica.

"Islands" was the name given to the PDDA morphology seen in Figure 3.5. The island morphology is made of disconnected islands of PDDA, where each island PDDA adopts the maze morphology. The island microstructure only appeared when mica substrates were used. The solution concentrations that were

used to form islands were approximately the same as those forming mazes, although islands were observed much less often than the mazes.

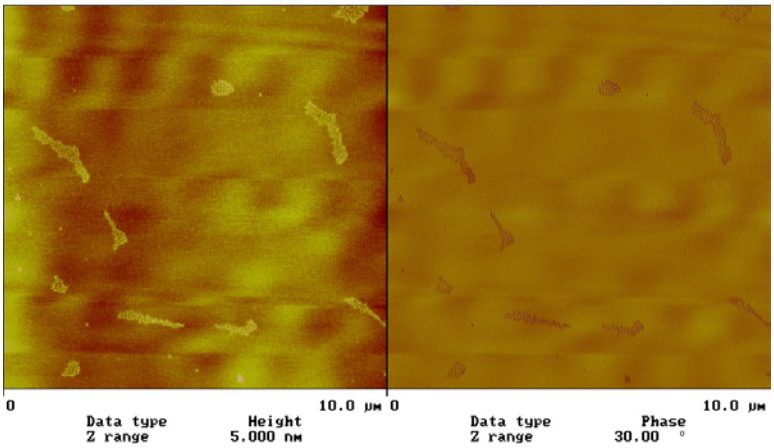

Figure 3.5: AFM height (left) and phase (right) images of a PDDA island morphology on mica.

The microstructure shown in Figure 3.6 was called the "needle" morphology, since the PDDA forms small needle like structures. Also present in Figure 3.6, but only visible on the height image on the left, are three circular height variations, called "haystacks". Haystacks were another microstructural feature that were sometimes present at high PDDA concentrations (HPDDA ≥ 5 w%). The phase image on the right of Figure 3.6 makes no distinguishment between haystacks and needles.

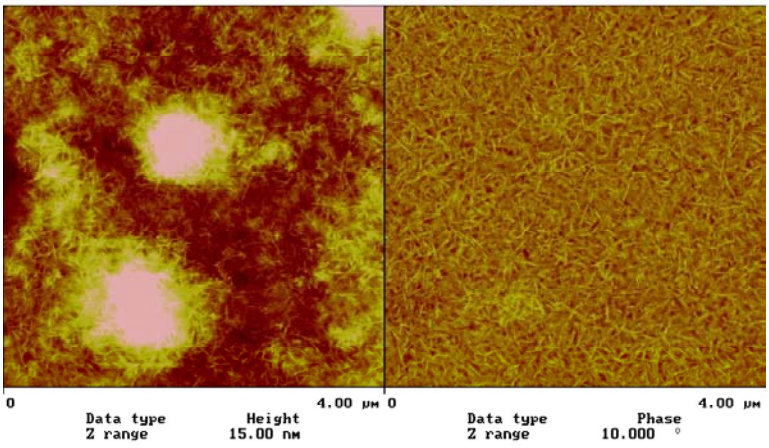

Figure 3.6: AFM height (left) and (right) phase images of the PDDA needle morphology on silicon.

The rods shown in Figure 3.7 were an unexpected result of the ISAM process. Rods appeared in HPDDA in concentrations as low as 5 w%, but were not observed in solutions less than 20 w% of LPDDA. It is unclear if the rods are actually cylinders, elongated hexagons, or rectangular. A length-wise section of a rod is given in Figure 3.8. The height of rods appear to be constant across their length.

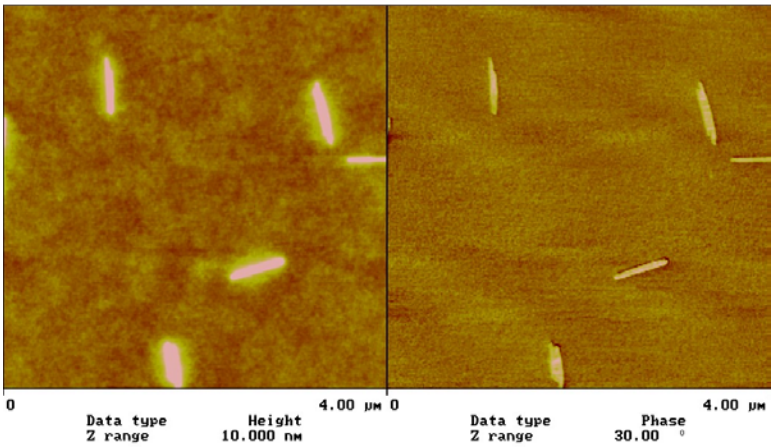

Figure 3.7: AFM height (left) and phase (right) images of rods on silicon.

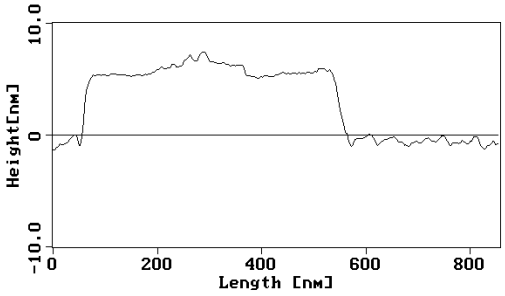

Figure 3.8: A length-wise section of a rod.

Table 3.2 gives a range of dimensions for the rods. Rods that appeared in films made with HPDDA solutions were generally larger than rods observed in films made with LPDDA solutions.

Table 3.2: Dimensional range of rods

	Length (± 25 nm)	Width (± 25 nm	Vertical (± 0.5 nm)	Aspect Ratios (± 0.5 l/w)
Min	125	50	3.0	2.3
Max	2300	250	7.0	9.0

Spherulites of PDDA were formed using 20 w% solutions HPDDA. Figure 3.9 shows an AFM phase image of PPDA spherulites. The spherulites have a diameter of approximately 2 μm. The AFM phase image in Figure 3.10 shows a rod serving as a spherulite nucleation site.

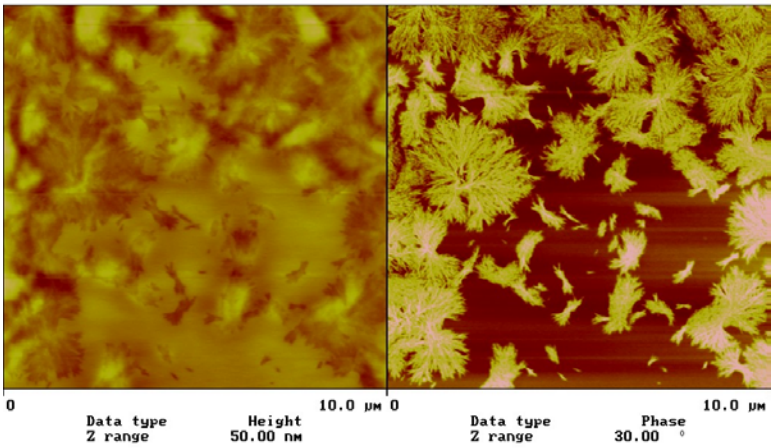

Figure 3.9: AFM height (left) and phase (right) images of PDDA spherulites on silicon.

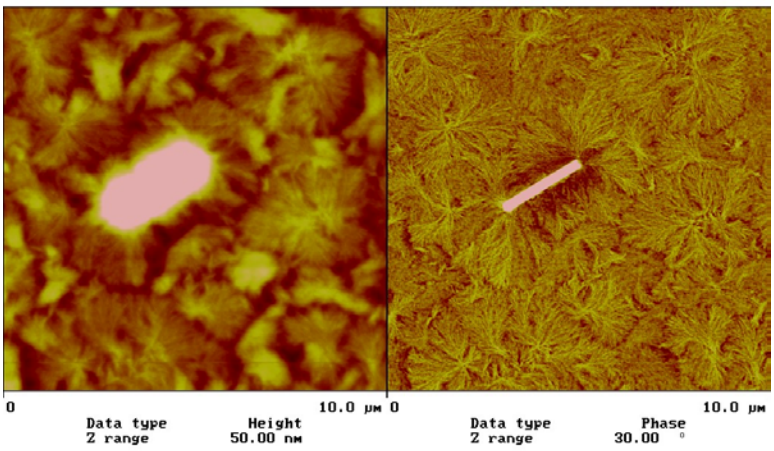

Figure 3.10: AFM height (left) and phase (right) images of PDDA spherulites nucleating out from a rod. The substrate was silicon.

The chart in Figure 3.11 shows the occurrence of PDDA morphologies as function of the PDDA solutions' concentrations and molecular weights. There is a higher propensity of HPDDA to form unusual microstructures than LPDDA. Solution concentrations in Figure 3.11 that fall between concentrations where microstructures were explicitly observed were also colored.

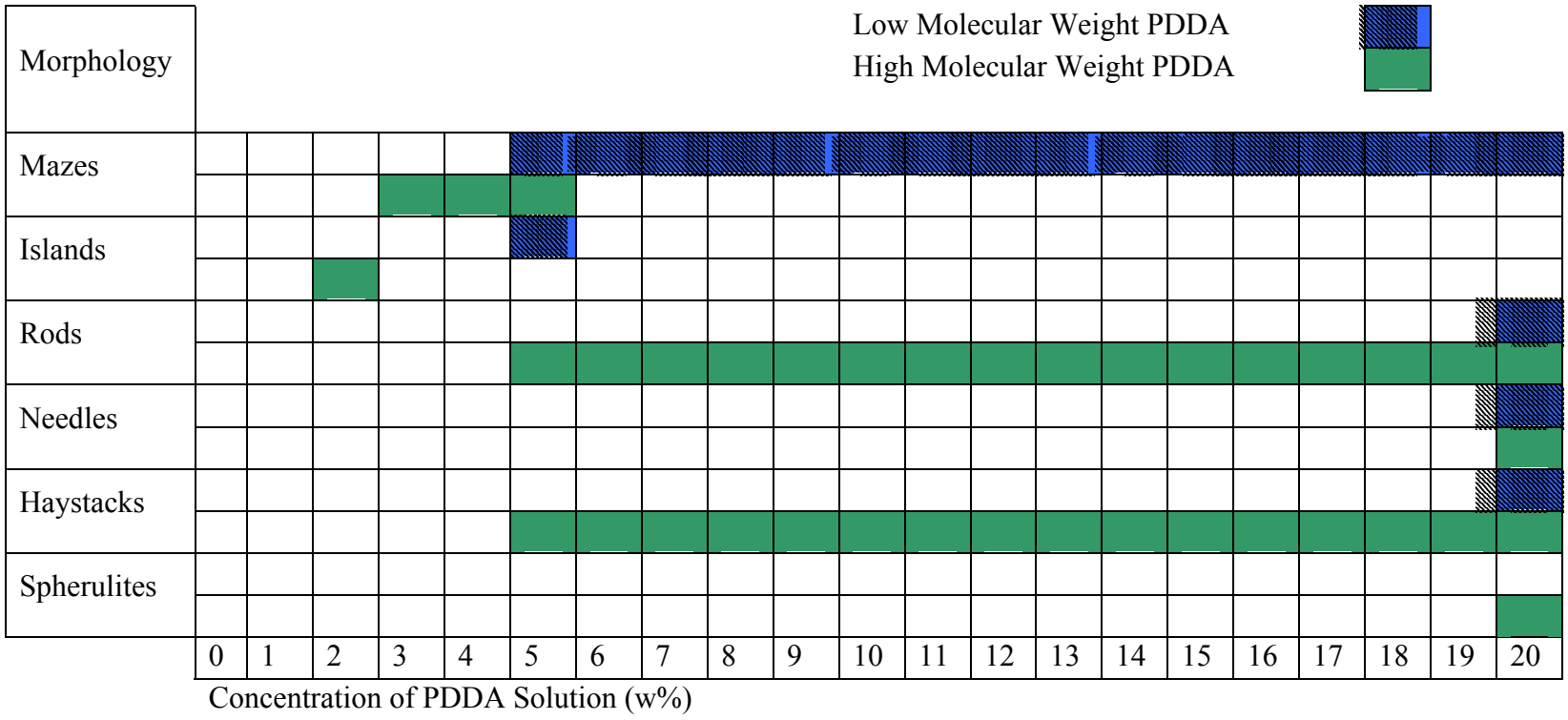

Figure 3.11: Graphical chart of different polymer morphologies present at different concentrations of PDDA

4. Unusual Montmorillonite Morphologies

Unexpected arrangements of montmorillonite were also observed. Figure 3.12 shows the montmorillonite sheets arranged in repeating rows, each approximately 1 micron apart. This same sample also had regions were the clay sheets were arranged randomly. Figure 3.13 shows stacks of laminated montmorillonite sheets approximately 75 – 100 nm high. These stacks of clay sheets were not sheared apart during processing at the vendor's facilities.

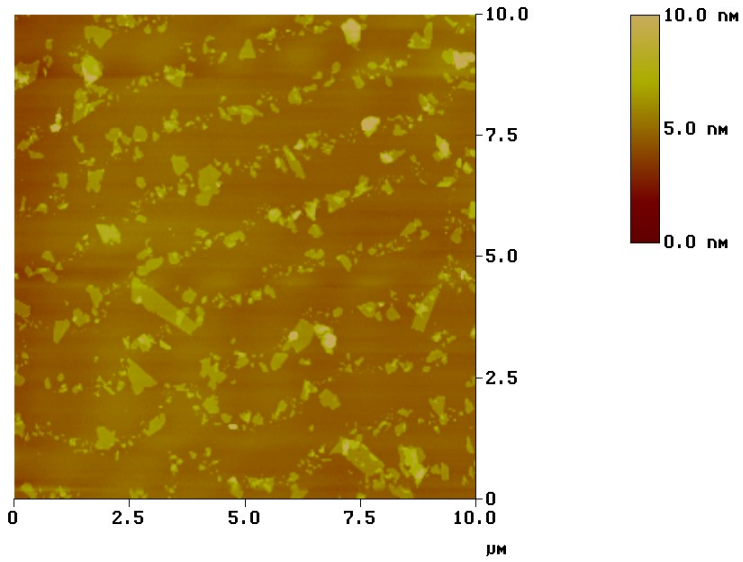

Figure 3.12: AFM height image of aligned montmorillonite platelets on a mica.

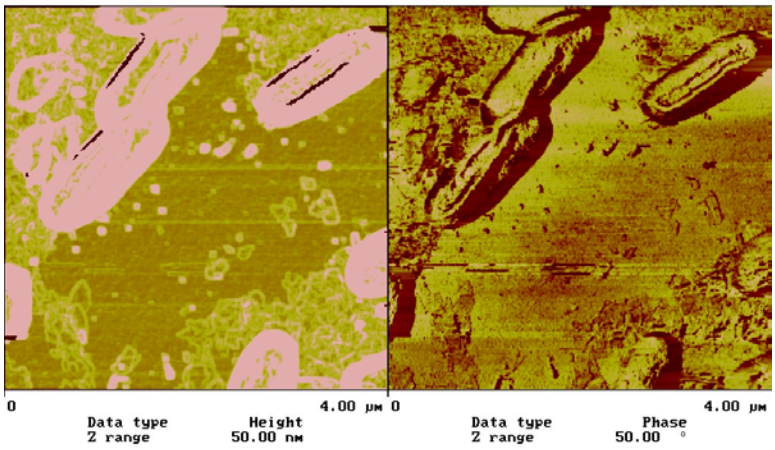

Figure 3.13: AFM height (left) and phase (right) images of clay platelets stacked on a mica.

5. Circular Patterns

Circular patterns of PDDA were unintentionally formed on the surface of silicon substrates provided by Wafer World Inc, Virginia Semi-conductor and MEMC Electronic Materials Inc. One circular pattern of Laponite and PSS was also made on silicon provided by Virginia Semi-conductor. The patterns, called "crop circles" and "stonehenges," for the PDDA and Laponite / PSS patterns, respectively, were almost without exception perfectly circular. The patterns' diameters varied between 2.8 – 0.12 μm. These patterns appeared only on silicon that was exposed to ultrasonic cleaning sometime during wafer preparation or ISAM deposition.

Crop circles were characterized by PDDA covering the surface of the silicon except certain circular regions. The outline of the PDDA around these regions formed a negative image of these regions, forming a crop circle. The interiors of the crop circles are the underlying silicon substrate, uncovered by the deposited PDDA. Typically, if crop circles were present on the surface of silicon at all, then crop circles covered more than 10% of the silicon's surface. A cluster of PDDA crop circles is shown in Figure 3.14. The overwhelming majority of the crop circles were circular, but an oblong crop circle was observed, and is shown in Figure 3.15.

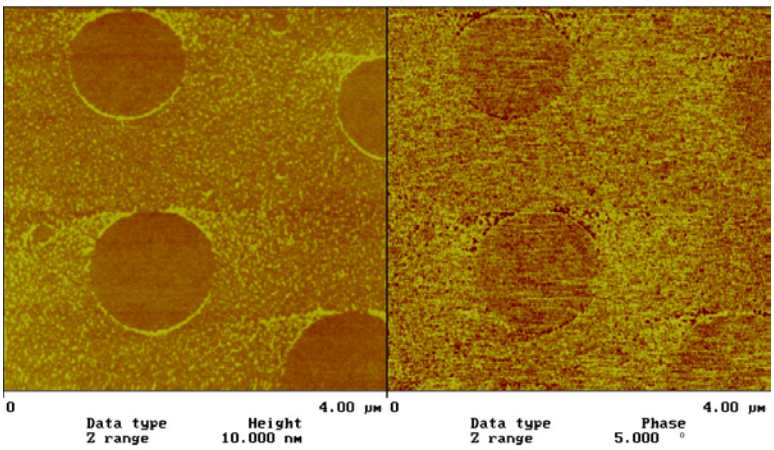

Figure 3.14: AFM height (left) and phase (right) images of crop circles on the surface of silicon.

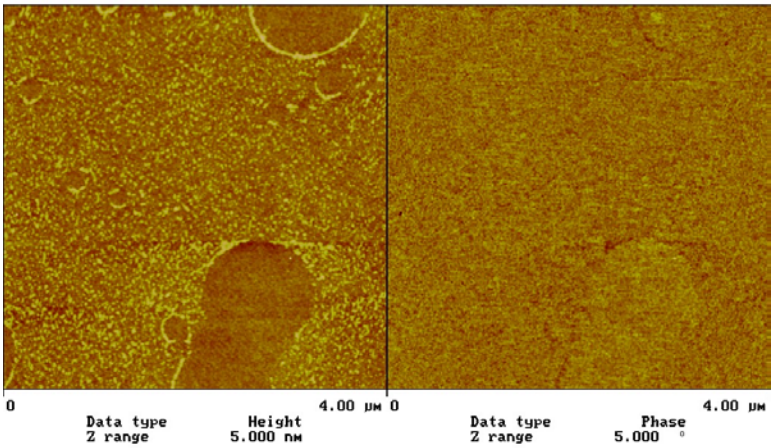

Figure 3.15: AFM height (left) and phase (right) images of a distorted crop circle on the surface of silicon.

Unlike crop circles, which were abundant on the surface of PDDA treated silicon, only one stonehenge was ever formed. A solution of 0.02 w% PSS and 0.02 w% Laponite was used to form the stonehenge is shown in Figure 3.16. The deposition sequence for forming the stonehenge is given in the Appendix.

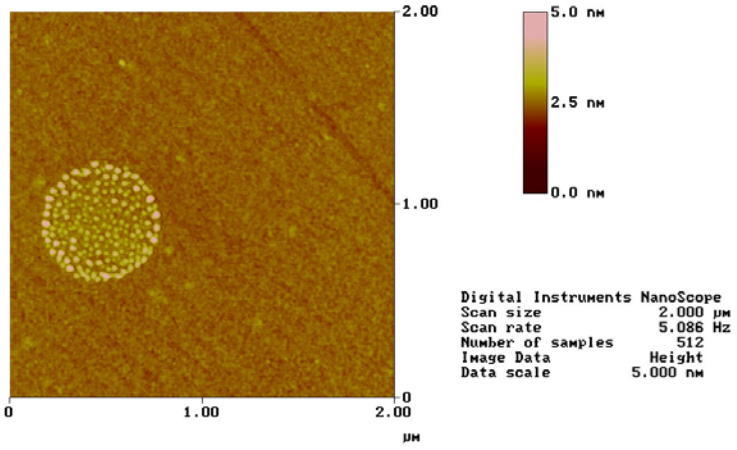

Figure 3.16: AFM height image of a stonehenge on the surface of silicon.

6. Intentionally Formed Circular Patterns

Although crop circles were initially produced by accident, a simple ISAM deposition sequence was developed to intentionally create crop circles on silicon using a 4.00 w% solution of HPDDA. Using one of the two listed techniques

(listed in the Appendix) crop circles were produced on silicon from Virginia Semi-conductor Inc, MEMC, and Motorola. AFM images of intentionally made crop circles are given in Figure 3.17 and Figure 3.18. There is no distinguishable difference between crop circles accidentally and intentionally formed.

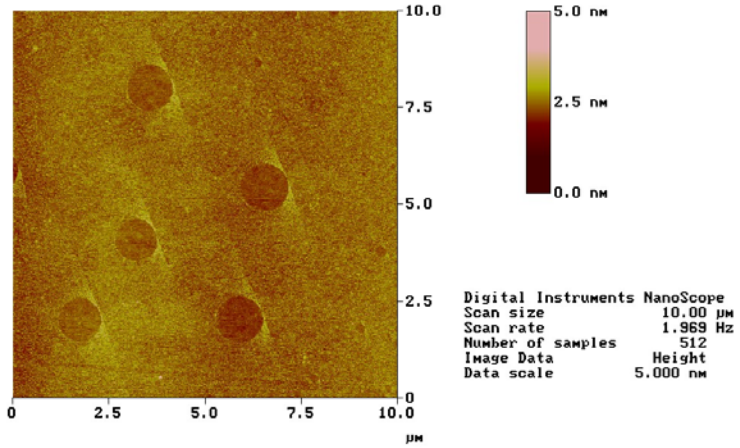

Figure 3.17: AFM height image of crop circles intentionally formed on the surface of silicon.

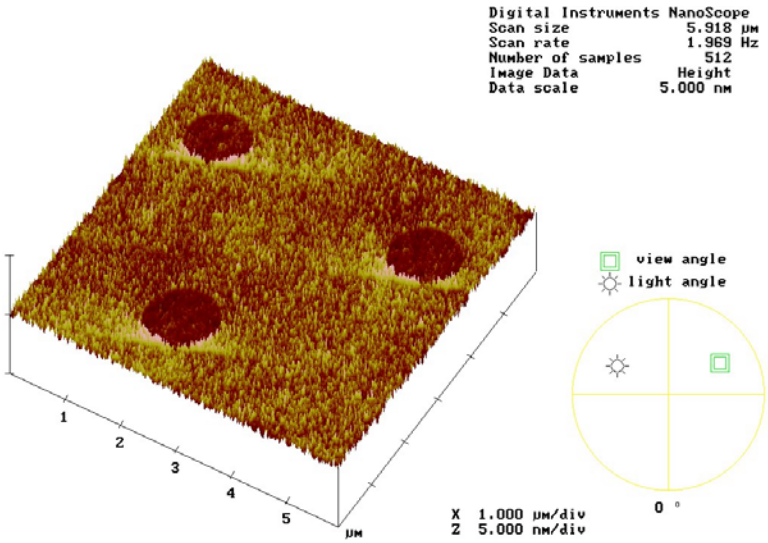

Figure 3.18: AFM height image of crop circles intentionally formed on the surface of silicon.

D. Discussion

1. Bare silicon

Silicon proved to be an ideal substrate for ISAM deposition. The wafers from all four vendors had average roughness less than 5 angstroms and were easily cleaved for ISAM use. The wafers did not cleave during ISAM deposition or nitrogen drying as did the previous mica substrates.

2. Overview of High Concentration PDDA Solutions

The unusual microstructures presented in this thesis indicate that when concentrations of PDDA are approximately 2.0 w% or greater, the ISAM technique breaks down and behaves like a dip coating process. At PDDA concentrations above 2.0 w%, the polymer is not entirely removed from the substrate during cleaning. Excessive polymer on the substrate then takes on a number of morphologies depending on solution concentration, molecular weight, and drying rate.

Kleinfeld and Ferguson reported controllable ISAM deposition of medium molecular weight PDDA using solutions of PDDA ≥ 5.0 w%. Kleinfeld and Ferguson, however, dripped their charged solutions onto a substrate, rather than submerging their substrate into solutions. Presumably then, dripping solutions onto a substrate rather then placing the substrate into solution reduces the amount of excessive polymer imparted onto the surface.

3. Mazes

It is hypothesized that excessive PDDA on the samples' surfaces is dewetting upon PDDA that is electrostatically bound to the substrate, generating maze-like morphologies. In a contact angle study, Kerle et al, coated a cross-linked film of

a diethylene / ethylethylene copolymer (DEco) with uncross-linked DEco.[38] The deposited DEco dewetted on the surface of the cross-linked and broke up into a polygonal network, shown in Figure 3.19, that is similar to maze-like morphologies of PDDA. During ISAM deposition, PDDA tightly binds to the oppositely charged substrate. If concentrations ≥ 4 w% PDDA are used however, excessive PDDA may still be present on the surface of the sample even after cleaning. The residual PDDA, laying on top of the PDDA anchored to the substrate, dewets, forming patterns similar to those in Figure 3.19. Every repeat unit of PDDA is positively charged, so it is unlikely that PDDA has a high affinity for self-adhesion between polymer chains, which would help promote dewetting of PDDA on a PDDA covered surface. Although the chemistries of DEco and PDDA are different, Kerle et al's work is a demonstration of polymer dewetting the surface of a like-polymer.

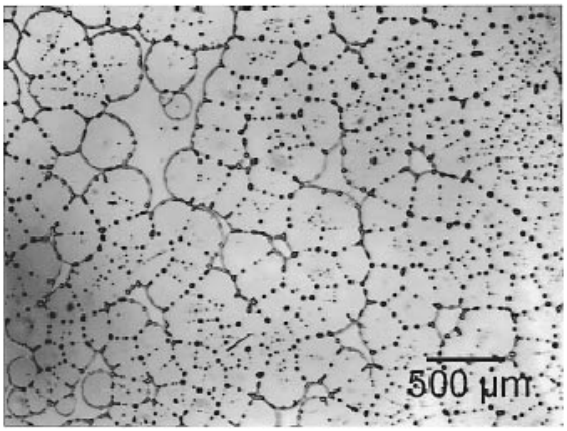

Figure 3.19: Uncross-linked DEco dewetting on the surface of cross-linked DEco.

The other source of maze formation is simple drying of the deposited PDDA / water film. As water evaporates from a PDDA / water film during drying, the concentration of PDDA left in the watery film continues to rise. Eventually, the concentration of PDDA in the deposited film is high enough to cause the PDDA

[38] Kerle, Tobias; Cohen, Sidney, R; Klein, Jacob. "Dihedral Angle at Solid/Liquid-Polymer Interfaces Determined by Atomic Force Microscopy." Langmuir. v13, n24, p6360, 1997.

to drop out of solution on the edges of evaporating water beads, leaving behind a maze-like pattern of PDDA.

4. Interpretation of Single Polymer Chains

The maze morphology gives the immediate impression that individual polymer chains form the branches seen in the maze. Work presented in this thesis suggests the branched patterns seen in PDDA maze morphologies are not single polymer chains, however. If the branches of a maze network were made of single polymer chains, then similar chains should have been observed beneath clay platelets in polymer / clay films in images shown throughout this thesis. Overlapping clay platelets, each ten angstroms high clearly reveal the contours of platelets beneath them, yet platelets, which are bound to the surface of the substrate, give no indication of the polymer chains being beneath them. Given that these "single chains" are approximately 5 angstroms high, their presence should clearly be identifiable on AFM images of polymer / clay films. In addition, these single chains are conspicuously missing from the sample given in Figure 2.11, which was a mica substrate coated with polymer and from Figure 2.31, a clay / polymer film terminated with polymer.

5. Islands

Islands are formed by the same mechanism as mazes, with the addition of mica cleavage. During deposition or cleaning, the surface of the mica cleaves away. Microdroplets of PDDA, near the sight of the cleavage, may be deposited on the freshly cleaved area of mica, either by being blown onto the cleavage site during N_2 drying, or loosely bound PDDA attaching itself to a newly available (and oppositely charged) site during a cleaning sequence. In either case, small deposits of PDDA, separated from one another, then proceed to take on the maze morphology.

6. Rods

The rod morphologies do not appear to be structures of PDDA. The phase image of the rod amidst the spherulites in Figure 3.10 shows that the elasticity of the rod and the surrounding spherulite are significantly different, so the rod is clearly not part of a PDDA spherulite, instead the rod appears to be acting as a nucleation sight for surrounding spherulites. The size of the rod in Figure 3.10 rules out the possibility that the rods are PDDA crystal lamellae. If rods are not made of PDDA, they are also too uniform in shape to be a form of dirt contamination. Rods are found in both low and high molecular weight solutions of PDDA. It is probable that the rods are by-products or residual synthesis compounds used in the manufacture of PDDA. Given that each solution of PDDA from Aldrich had a Mw range ≥ 100 kg/mol it seems unlikely that a great deal of extra care was used in the manufacture of the PDDA solutions. Hence, it would not be surprising that the PDDA solutions contain some impurities. The synthesis of diallydimethyl-ammonium salts is briefly discussed in the Polymer Handbook.[39]

7. Needles, Haystacks and Spherulites

The phase image in Figure 3.6 shows that the mounds, or "haystacks", in the corresponding height image are structurally identical to the surrounding needles. Clearly then, haystacks are agglomerations of needles. Needles and haystacks are probably a pre-spherulitic structure of PDDA. The presence of spherulites in Figure 3.9 and Figure 3.10 clearly demonstrates the ability of PDDA to crystallize.

8. Reproducibility of Unusual Polymer Morphologies

Since all of the unusual PDDA morphologies were created accidentally, the repeatability of these results is somewhat questionable. Future research in this

[39] J. Brandup; E.H. Immergut; Grulke, E; ed. Polymer Handbook: 4th edition. Wiley-Interscience. 1990.

area should use the ISAM deposition sequences listed in the Appendix as a guide to help create these morphologies. The number of different dipping sequences that resulted in each of these morphologies is indicative of how difficult it is to purposely create these morphologies.

9. Unusual Montmorillonite Patterns

Originally, the alignment of the clay platelets in Figure 3.12 was thought to have been caused by the AFM tip running across the surface of the substrates. Attempts to use the AFM tip to create rows of platelets failed, however. It is possible that the ultrasonic agitation used to clean the sample was enough to shake polymer chains attached to the mica into ordered rows, clay attached to the PDDA followed as well. Low concentrations, 0.02 w%, of both PDDA and clay were used to make the sample in Figure 3.12. The lack of deposited PDDA probably aided in the patterning process. If the entire surface of the mica had been saturated with copious amounts of PDDA, the motion of polymer caused by the ultrasonics would have been impeded by polymer already present. The alignment of the platelets in Figure 3.12 should not be considered experimentally repeatable.

The clay solutions that were provided by SCP and Nanocor Inc. underwent high shear during processing in order to delaminate individual clay sheets from each other. The image in Figure 3.12 indicates that not all of the clay sheets were delaminated from one another. The existence of the stacked clay platelets shows that the Closite® solutions still contains stacks of clay platelets.

10. Crop circles and Stonehenges

AFM images of crop circles and stonehenges indicate that circular regions of positive charge can be produced on the surface of silicon. In the case of crop circles, PDDA deposits around, but not in these regions of charge. The like-charge of the circles and PDDA repel each other, forming a negative image of the charged areas. Stonehenges are the reverse of crop circles, negatively charged

clay platelets avoid the negatively charge silicon substrate and attach themselves only to the positively charged regions.

Ultrasonic cleaning of silicon causes these regions of charge. When the silicon substrates are ultrasonically cleaned, bubbles form and explode on the silicon's surface which either damages the silicon's oxide layer or the hydroxyls attached to the oxide layer. The oxide layer is *not stripped away*, as usually the native oxide of silicon is ~ 20 nm thick. A depression 20 nm thick would have been easily noticeable on the AFM image of the stonehenge. In any event, the damaged oxide layer assumes a positive charge that repels PDDA and attracts Laponite and PSS. The reason behind the charge reversal is purely speculative, hydroxyl groups trapped within the exploding bubble may have become protonated, or perhaps the damaged oxide layer assumed a different level of hydration which altered the oxide's charge.

The oblong shape of the crop circle in Figure 3.15 was probably caused by the washing and N_2 drying of the substrate. The cleaning process may have simply redeposited some of the PDDA at the edges of the crop circle in the direction of N_2 gas or of the cleaning water.

E. Conclusion

Using concentrations of PDDA above 2 w% causes the breakdown of the ISAM process, as excessive PDDA is deposited on the surface of the substrate that is not removed during cleaning. The extra PDDA on the surface of the substrate often forms branched patterns of polymer that form maze-like morphologies. The individual branches of these mazes are not single chains of polymer, but rather agglomerations of PDDA. The formation of these patterns may be a type of dewetting. Rapid drying using N_2 and the ionized nature of PDDA may aid in the dewetting process. Rod shaped structures, believed to be residual compounds used in the synthesizing of PDDA exists in solutions of the polymer. Pre-spherulitic structures of PDDA have a needle-like morphology; these needles tend to

agglomerate into larger mounds, called “haystacks.” High molecular weight PDDA was crystallized; the average spherulite size was approximately 2 μm in diameter.

Laminated stacks of montmorillonite were found in the Closite ® solution provided by SCP. The silicate stacks were made from over 100 single clay sheets. It was found that ultrasonic agitation could produce crude patterns of montmorillonite platelets.

Bubbles at surface of silicon wafers made by ultrasonic cleaning create circular regions of positive charge. These areas of charge can be detected by placing wafers into solutions containing negatively or positively charged solutions of clay or polymer, respectively.

CHAPTER 4: CORROSION RESISTANCE ON 2024-T3 AL

A. Introduction

1. Corrosion of 2024-T3 Al alloys

The addition of alloying elements in aluminum to form high strength alloys such as 2024-T3 also makes these alloys vulnerable to corrosion.[40] In service, 2024-T3 Al corrodes through a number of mechanisms, two of which will be overviewed, IGC-exfoliation, and pitting.

Intergranular corrosion (IGC) in 2024-T3 alloys is the result of an internal galvanic couple. Copper-aluminide precipitates exist along grain boundaries in 2024-T3. Areas neighboring the precipitates are copper-poor, while the bulk metal is relatively copper-rich; a schematic showing 2024-T3's microstructure near a grain boundary is given in Figure 4.1.

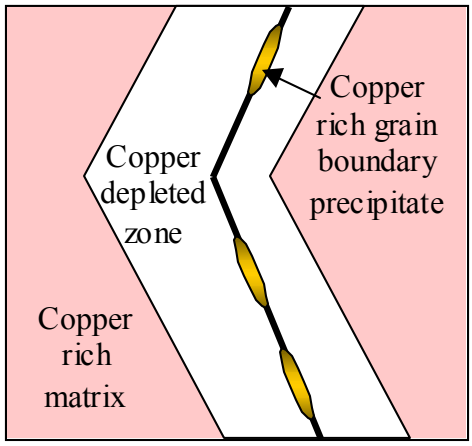

Figure 4.1: Schematic of grain boundary region in a 2XXX alloy.[41]

The copper-poor areas along the grain boundaries and the copper-rich phase of the surrounding metal form a galvanic couple with a potential difference of

[40] Morris E. et al. "Evaluation of non-chrome inhibitors for corrosion protection of high-strength aluminum alloys." Polymeric Materials Science and Engineering: Fall Meeting, New Orleans, Louisiana, USA, 22-26. v81, p167, Aug 1999.

[41] Image based on Schweitzer, Phillip A, ed. Corrosion Engineering Handbook. Marcel Dekker, Inc. New York, NY. 1996. (Courtesy of ALCOA Technical Center, Edwin L. Colvin.)

about 0.12 Volts.[42] When IGC occurs, the "entrapped corrosion product is about five times as voluminous as the metal consumed."[42] In a rolled alloy where the grain structure is aligned, the build of corrosion products separates layers of the metal from one another, producing a peeling effect. This particular form of IGC is called "exfoliation". Exfoliation corrosion occurs in both industrial and marine atmospheres.

Pitting corrosion is also an issue with 2024-Al alloys, particularly in marine environments. Pitting is a localized form of corrosion that creates small holes, or "pits" on the surface of materials. Imperfections present on the oxide surface usually act as initiation sites for pitting. As general corrosion affects the aluminum alloy, copper corrosion products form on the exterior of the pits. With more noble corrosion products on the outside of the pit, the interior of the pit becomes the anode while the exterior becomes the cathode in a galvanic couple. Besides copper compounds, other corrosion products, usually aluminum oxide and aluminum hydroxide are also deposited outside the pit. Cloride ions are a known promoter of pitting corrosion.

2. Chromate Conversion Coatings

Although a number of anti-corrosion treatments can be performed on aluminum, chromate conversion coatings (CCCs) are "generally considered to give the best corrosion resistance and are specified for use in military applications."[43] CCCs are produced on several types of metals, the most common being aluminum, magnesium, and copper alloys. CCCs are formed on these metals by immersing them in an acidic bath of chromate and fluoride. The

[42] Schweitzer, Phillip A, ed. Corrosion Engineering Handbook. Marcel Dekker, Inc. 1996.

[43] Bibber, John W. "A Chrome-Free Conversion Coating for Aluminum with the Corrosion Resistance of Chrome." Corrosion Reviews. p303, v15, n3-4, 1997.

resulting film contains both trivalent and hexavalent chromium. The exact mechanism of how CCCs impede corrosion is not known.[44]

However, it is "generally believed that CCC formation involves destabilization of the passive oxide film by fluorine, followed by reduction of chromate to the exposed aluminum."[45] Depending on hydration states and charge, one possible mechanism for CCC formation is shown in Equation 4.1.[45]

Equation 4.1: $2Al + Cr_2O_7^{-2} + 8H^+ \Leftrightarrow 2Cr(OH)_3 + H_2O + 2Al^{+3}$

Chromate coatings that have been scratched still exhibit corrosion protection, "because the hexavalent chromium content is slowly leachable in contact with moisture".[45] This self-healing property of CCCs makes their application for corrosion protection particularly attractive.

3. Chromate Conversion Coating Replacements

Unfortunately, the use of CCCs is limited by the extreme toxicity of chromium, "due to its very toxic nature, chromium is on the EPA's list of the 17 most hazardous materials and is targeted for elimination from the work place."[46] A wide variety of non-chromium based corrosion protection schemes have been proposed or utilized, including cerium nitrate, conductive polymers and phosphate conversion coatings.[4346-49] In particular interest to this thesis are ceramic platelet

[44] Zhao, J; Frankel, G; McCreery, RL. "Corrosion protection of untreated AA-2024-T3 in chloride solution by a chromate conversion coating monitored with Raman spectroscopy." Journal of the Electrochemical Society, v145, n7, p2258. July 1998.

[45] Eppensteiner, Fred W. and Jenkins, Melvin R. "Chromate Conversion Coatings." Metal Finishing 66th Guidebook and Directory Issue. v95, n1, p489, Jan 1998.

[46] Buchheit, R.G; Brode, M.D; Stoner, G.E. "Corrosion-Resistant, Chromate-Free Talc Coatings for Aluminum." Corrosion. v50, n3, p205, March 1994.

[47] Sitaram, S.P; Stoffer, J.O; O'Keefe, T.J. "Application of Conducting Polymers." Journal of Coatings Technology. v69, n866, p65. March 1997.

[48] "Conducting Polymers and Corrosion: Part 2-Polyaniline on Aluminum Alloys." Tallman, D.E; Pae, Y; Bierwagen, G.P; Corrosion. v56, n4, p401. April 2000.

reinforced coatings and potassium aluminum silicate conversion coatings. Corrosion resistant coatings reinforced or consisting of ceramic platelets provide the advantage of creating a lengthened diffusion path for corrosion promoters, such as for the Cl^- anion shown in Figure 4.2.

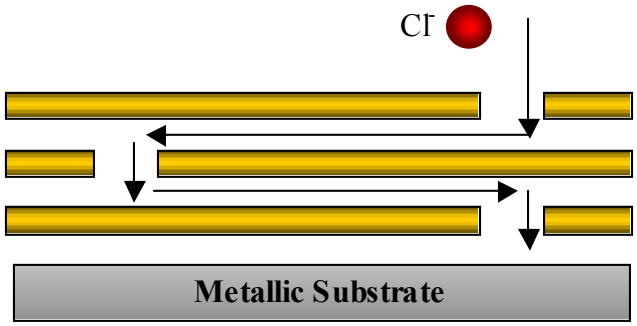

Figure 4.2: Lengthened diffusion path of a Cl^- anion caused by the incorporation of ceramic platelets into a corrosion resistant coating.

At least two examples of corrosion resistant coatings composed of platelets exist in literature. In the study by Buchheit et al. lithium aluminum hydroxide carbonate hydrate- $Li_2[Al_2(OH)_6]_2 \bullet CO_3 \bullet nH_2O$, was precipitated out on the surface of aluminum alloys.[46] In this novel approach the proposed coating was formed using environmentally benign chemicals. Corrosion resistance offered by the film however was considerably poorer than that provided by CCCs.

Mica has been shown to improve the corrosion resistance offered by coatings on steel as early as the 1950's.[50] Mica, incorporated into coatings acts as a physical barrier to the permeation of corrosion promoters as shown in Figure 4.2. It has been shown experimentally that corrosion resistant films that incorporate mica improve with increasing mica platelet aspect ratios.[50]

Other conversion coatings have also been investigated as possible replacements for CCCs. In the conversion coating outlined by Bibber, aluminum oxide is converted into a potassium aluminum silicate using relatively benign

---

[49] Wernick, S; Pinner, R; Sheasby, P.G. The Surface Treatment and Finishing of Aluminum and its Alloys, v1, 5th ed. ASM International. 1987.

[50] Gee, S. "Water-borne coatings for steel." JOCCA-Surface Coatings International. v80, n7, p316. July 1997.

chemicals.[43] The resulting silicate film offers substantial corrosion resistance on Al alloys.[43] ISAM deposition has already been demonstrated on another potassium aluminum silicate, mica. Any ISAM films developed for corrosion resistance could conceivably be added on top of already corrosion resistant potassium aluminum silicate films.

Dr. Bruening's group at Michigan State University has done the only recorded application of ISAM films for corrosion resistance to date.[51] In their work, Dr. Bruening's group formed ISAM films of polyacrylic acid and dechlorinated polyallylamine hydrochloride to cover aluminum sputter coated silicon wafers. Once the films were formed they where heated in a nitrogen atmosphere to crosslink the polyelectrolytes and form a polyimide. Electrochemical data on the polyimide films indicated that the films might provide significant corrosion protection to the underlying aluminum.

B. Procedure

3" x 1" x 0.63" coupons were machined from a 0.63" thick sheet of 2024-T3 Al purchased from McMaster-Carr and then cleaned using one of the three following techniques.

1. Simple Methanol Wash

Coupons of 2024-T3 Al were ultrasonically cleaned in methanol for 30 minutes using a 5510 Branson Ultrasonic Cleaner. Dark smudge marks appeared on some of the samples. Attempts to remove the marks using acetone and deionized water failed. Samples cleaned using this method will not have any subscript attached to them. The coupons were then air dried and kept in a Sanpla Drykeeper dry cabinet until use.

[51] Dai, Jinhua; Sullivan, Daniel M; Bruening, Merlin L. "Ultrathin, Layer Polyamide and Polyimide Coatings on Aluminum." Industrial Engineering Chemical Research. v39, n10, p3528. 2000.

2. Sand Blast with Improved Methanol Wash

Coupons were sandblasted to remove the native oxide and any surface contaminants. Samples that have been sandblasted will have the $_{sb}$ subscript attached to them for this report. After sandblasting, the samples were exclusively handled with gloves at all times, to prevent surface contamination from skin oils. The samples were then ultrasonically cleaned with a 5510 Branson Ultrasonic Cleaner in a bath of deionized water for 30 minutes. After cleaning with deionized water, the samples were rinsed with tap water while being rubbed by hand. Then the samples were ultrasonically cleaned in methanol for 30 minutes and were again rinsed with tap water while being rubbed by hand. Finally, selected 2024-Al alloy coupons were placed in a glass beaker of boiling deionized water for 15 minutes to form a ~ 300 nm thick oxide / hydroxide layer; these samples will have an $_{sb/ox}$ subscript attached to them throughout this report.[43] Coupons that were boiled in the deionized water turned a steel gray color. All of the samples were blown dry with N_2 and kept in a Sanpla Drykeeper dry cabinet until use.

3. Acid Wash

A third cleaning procedure was also developed. Machined samples were degreased in methanol using a Fisher Scientific F560 Ultrasonic Cleaner for 30 minutes and allowed to air dry. The samples were then etched for three minutes in a heated acid solution to remove their oxide coating; some residual methanol may have been on the coupons' surfaces before being placed into the acid etch.[52] The acid solution consisted of (50 mL 96% H_2SO_4, 25 mL 70% HNO_3, 425 mL, deionized water). The temperature of the acid bath ranged from 65 – 80 ^oC. After being etched the samples were dipped into a 500 mL beaker of deionized water and were rinsed with deionized water while being rubbed by hand. The coupons were then boiled in deionized water for 15 minutes, wiped dry using Kimwipes,

[52] Van Horn, Kent R. Aluminum Vol III: Fabrication and Finishing. American Society for Metals. 1967.

and stored in a Sanpla Drykeeper dry cabinet until use. Coupons that underwent this cleaning procedure will have an $_{acid}$ subscript attached to them for this report.

4. Preparing ISAM solutions

a) Ultem solutions

Half a gram of an Ultem-type polyamic acid salt (Ultem) was donated as a gift from Dr. RM Davis, (Chemical Engineering, Virginia Tech) after being synthesized by Dr. JS Riffle, (Chemistry, Virginia Tech).[53] Ultem® is a thermoplastic available from General Electric; the polyelectroylte used in this study has a similar composition and will be referred to as "Ultem" for this report. Figure 4.3 shows the repeat unit of Ultem before and after thermal imidization.

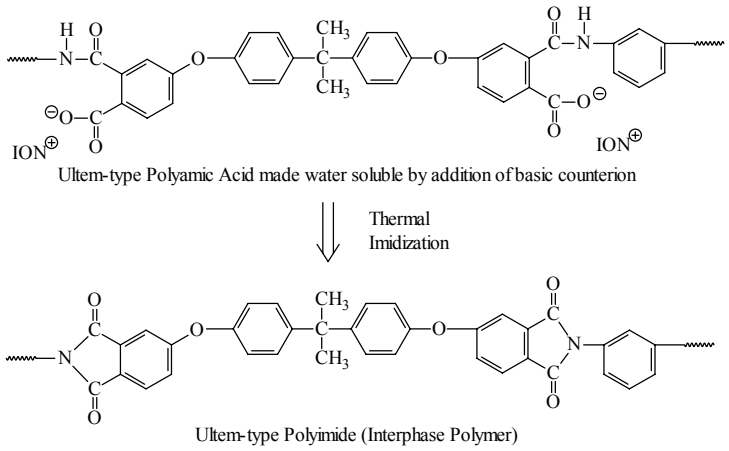

Figure 4.3: Repeat unit of the Ultem-type polyamic acid, before and after imidization

A 98% solution of Tripropylamine (TPA) was obtained from Aldrich and a 0.25 M solution of TPA was mixed using deionized water. Although the toxicity of the TPA is low, it should be handled under a fume hood, due to its pungent odor. A 10 mol^{-3} solution of Ultem was then mixed using the 0.25 M

[53] Facinelli JV; Gardner SL; Dong L; Sensenich CL; Davis RM; Riffle JS. "Controlled molecular weight polyimides from poly(amic acid) salt precursors." Macromolecules, v29, p7342, Nov 4, 1996.

solution of TPA. Finally, the Ultem solution was filtered with VWR 413 quantitative filter paper to remove trace amounts of undissolved Ultem. The resulting 10 mol^{-3} solution of Ultem was placed into a Coplin staining jar and stored in a refrigerator until use. The pH of the Ultem solution was maintained at 8.0 using TPA at all times. At a pH below 8.0, hydrolysis of the polymer chains may occur, detrimentally affecting the polymer. Tripropylamine (TPA) is the only additive that should be used to maintain a basic pH of an Ultem solution[54].

b) Other solutions

Other ISAM solutions of polyarylic acid (PAA, M_w = 100 $kg.mol^{-1}$, Aldrich), polyallylamine hydrochloride (PAH, M_w = 70 $kg.mol^{-1}$, Aldrich), polyethylenimine (PEI, M_w = 85 $kg.mol^{-1}$, Aldrich), and Laponite were prepared using deionized water. The PAA and PEI supplied by Aldrich were in 35 w% and 50 w% solutions, respectively. The repeat units of the polyelectroyltes are given in Figure 4.4 - Figure 4.6. The Laponite solution should be kept stirred until use, to prevent Laponite from settling out of solution. A 10 mol^{-3} solution of PAH was mixed using TPA to adjust its pH, unfortunately the TPA caused PAH to drop out of solution forming gelatinous precipitates. As a result of the TPA / PAH reaction, this solution was never used to form a protective ISAM coating.

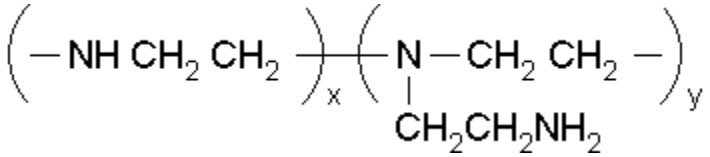

Figure 4.4: Repeat unit of polyethylenimine (PEI)

[54] Private communication with Professor R Davis, Chemical Engineering, Virginia Tech.

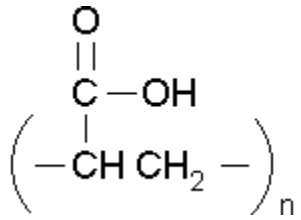

Figure 4.5: Repeat unit of polyacrylic acid (PAA)

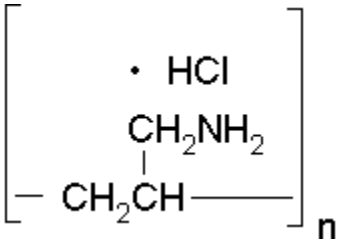

Figure 4.6: Repeat unit of polyallylamine hydrochloride (PAH)

5. ISAM film deposition

Immediately prior to deposition, the pHs of ISAM solutions were measured using an Accumet ® AR15 pH meter. The pH of PAA and PAH solutions were adjusted using HCl and NaOH. The pH of PEI and Lap solutions were never adjusted. The coupons were coated with the ISAM solutions following a standard procedure (Appendix) with deposition times of 5 minutes. During ISAM deposition of the (PAA / PAH) film, pitting was observed on the 2024_{sb} coupon. After deposition was completed, a single drop of TPA was usually added to the Ultem solution to maintain the solution's basic pH. Sixty individual layers of material were deposited on each coupon. For coatings that did not contain Laponite, 60 individual layers of material was the equivalent of 30-bilayers. The coatings that contained Laponite consisted of 5-bilayers of (Ultem / PEI) (for a total of ten separate layers) followed by a sequence of (Lap / PEI / Ultem / PEI) until an additional 50 layers of either polymer or Laponite were placed on the coupons. The aluminum coupons were assumed to have a positive charge (Appendix).

6. Curing of ISAM films

Aluminum samples with a (PAA / PAH) coating were placed into a 282A Fisher Scientific Isotemp Vacuum Oven at room temperature. The oven was alternately purged with a vacuum (9 inches of Hg) and N_2 gas (25-30 inches of Hg) five times. The oven was then heated to 215^{o}C for two hours under a steady flow of N_2 gas (25-30 inches of Hg). After heating, the samples were allowed to oven cool overnight in a N_2 atmosphere (25-30 inches of Hg). The coupons were then delivered to Litton Polyscientific Inc. for salt spray testing.

Coupons with an (Ultem / PEI) or (Ultem / PEI / Lap) coating were placed into a glass slide holder inside an AIM Hi-Temp 8817 oven and heated following the temperature ramp diagram given in Figure 4.7. Coupons were oven cooled until they reached 90^{o}C.

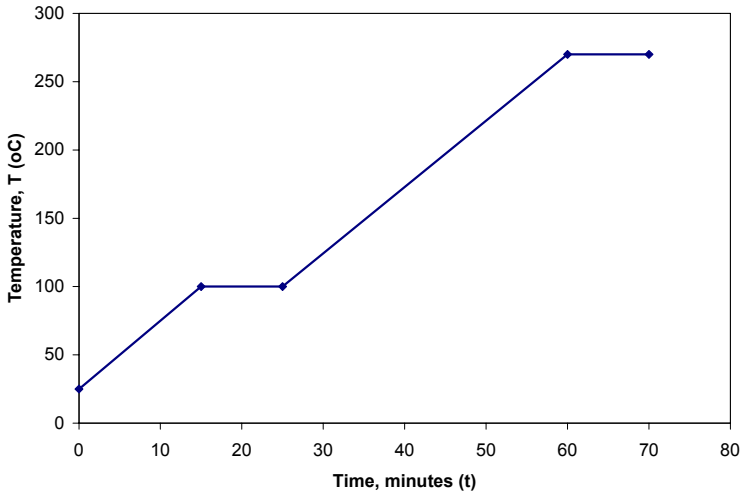

Figure 4.7: Heating diagram for Ultem-based ISAM films

7. Salt Spray Testing

Prepared coupons were delivered to Litton Polyscientific Inc. and submitted to a standard ASTM B117 salt fog test for 168 hours (one week). In order to keep track of the samples, a technician at Litton Polyscientific Inc. applied adhesive labels to the backs of the samples as necessary.

8. Samples prepared for AFM

Phosphorus doped, N-type, (100) silicon wafers were purchased from Virginia Semiconductor Inc; the wafers were scribed and cleaved into 1 x 7 cm pieces using a diamond scribe. The silicon coupons were then cleaned with deionized water in a 5510 Branson Ultrasonic Cleaner for 1 minute. ISAM films of (Ultem / PEI) and (Ultem / PEI / Lap) were deposited onto the wafer sections using deposition times of 5 minutes. The pH of the PEI, Ultem, and Lap were (8.6, 9.2, and 9.4 ± 0.1), respectively. The deposition of the polyelectroyletes and Laponite are given in Table 4.1. Repeated dipping in the solution of PEI for the first 4 deposition steps was an attempt to prevent the formation of "crop circles" on the surface of the silicon.

Table 4.1: Deposition of polyelectroytles and Laponite RD® on Si wafers.

Deposition step	(Ultem / PEI) sample	(Ultem / PEI / Lap) sample
1-4	PEI	PEI
5	Ultem	Ultem
6	PEI	PEI
7	Ultem	Lap

After deposition was completed the samples were blown dry with N_2 and heated to 270^{o}C to imidize the Ultem polymer using the temperature ramp given in Figure 4.7. After cooling, the samples were cleaved into 1 x 1 cm sections and adhered to AFM mounts. N_2 gas was used to remove any residual particles of silicon that were on the surface after cleaving the samples. The samples were viewed using an AFM in tapping mode.

9. Thermogravimetric analysis of polyethylenimine

Thermogravimetric analysis (TGA) was performed on a 33.2 mg sample of 50 w% PEI solution. The sample of PEI was heated in air using the same temperature ramp given in Figure 4.7 using a Perkin-Elmer TGA 7

thermogravimetric analyzer. After TGA of the sample was complete using the fore mentioned temperature ramp the sample was heated until it vaporized.

C. Results

1. Corrosion Test Results

The results of 168 hours of salt spray testing on 2024-Al alloy coupons are given in Table 4.2. All of the uncoated coupons failed; their surfaces were completely covered with corrosion products and pit marks. The performance of the samples was measured qualitatively. Images of the samples are given in the following figures.

Table 4.2: 60 layer thick corrosion resistant ISAM coating applied 2024-T3 Al.

Coating System:	PAA /PAH	PEI / Ultem	PEI / Ultem / Lap
Concentration (10^{-3} mol)	10 / 10	10 / 10	10 / 10 / 0.02 w%
Al-2024 (pH / pH)	Poor (5.5 / 5.5)	Good (9.8 / 9.3)	Good (8.6 / 9.4 / 9.2)
$Al\text{-}2024_{sb}$ (pH / pH)	Failed (5.5 / 5.5)	Failed (9.4 / 9.3)	N/A
$Al\text{-}2024_{sb/ox}$ (pH / pH)	Failed (5.5 / 5.5)	Moderate (9.8 / 9.3)	Moderate (8.6 / 9.4 / 9.2)
$Al\text{-}2024_{acid}$ (pH / pH)	N/A	Good (9.2 / 9.2)	Good (9.9 / 9.3 / 8.2)

Coupons of 2024-T3 Al alloy that were cleaned with the simple methanol wash after 168 hours of salt spray testing are shown in Figure 4.8. Significant pitting corrosion was observed on the (PAA / PAH) coated coupon. The (PEI / Ultem) and (PEI / Ultem / Lap) coated samples had discolorations and several pits on their surface but otherwise demonstrated corrosion resistance. The heavy

corrosion at one end of each ISAM covered coupon was due to the ISAM solutions not completely covering the samples during dipping.

Figure 4.8: 2024-Al samples cleaned only with methanol after salt spray testing. Left to right: Uncoated, (PAH / PAA), (PEI / Ultem), (PEI / Ultem / Lap)

All of the samples of 2024-T3 Al alloy that were sandblasted and left unoxidized failed, regardless of their coating, after being exposed to 168 hours of salt spray testing, as shown in Figure 4.9.

Figure 4.9: Sandblasted, unoxidized 2024-Al samples after salt spray testing. Left to right: Uncoated, (PAH / PAA), (PEI / Ultem)

Salt spray tested samples of 2024-T3 Al alloy that were sandblasted and oxidized are shown in Figure 4.10. All of these coupons were more corrosion resistant than their unoxidized counterparts. The (PEI / Ultem) and (PEI / Ultem / Lap) coated samples showed improved performance over the uncoated samples. Again, the corrosion at the tops of the (Ultem / PEI) and (Ultem / PEI / Lap) covered coupons was due to the ISAM solutions not completely covering the samples during dipping.

Figure 4.10: Sandblasted, oxidized 2024-Al samples after salt spray testing. Left to right: Uncoated, (PAH / PAA), (PEI / Ultem), (PEI / Ultem / Lap)

Salt spray tested samples of 2024-T3 Al alloy that were acid etched and oxidized are shown in Figure 4.11 through Figure 4.13. Corrosion pits were present on all of the (PEI / Ultem) and (PEI / Ultem / Lap) coated samples. Each of these samples showed a substantial improvement over the uncoated samples, however. The (PEI / Ultem) coated samples retained their luster better than the (PEI / Ultem / Lap) coated samples, but the (PEI / Ultem) coated samples also had more pit marks on them.

Figure 4.11: Front and back of acid etched, oxidized 2024-Al samples after salt spray testing. Uncoated samples

Figure 4.12: Front and back of acid etched, oxidized 2024-Al samples after salt spray testing. (PEI / Ultem) samples

Figure 4.13: Front and back of acid etched, oxidized 2024-Al samples after salt spray testing. (PEI / Ultem / Lap) samples

2. AFM of Ultem based coatings

ISAM films of (Ultem / PEI) and (Ultem / PEI / Lap) that were deposited onto sections of silicon wafer and viewed using AFM are shown in Figure 4.14-Figure 4.16. Images produced by an AFM show a contrast between the (Ultem / PEI) coating, and the (Ultem / PEI / Lap) coating. Laponite platelets are clearly visible in the (Ultem / PEI / Lap) coating and form a nearly continuous silicate barrier across the surface of the substrate. What appears to be a residual "crop circle" on the (Ultem / PEI / Lap) coating is pointed in Figure 4.16.

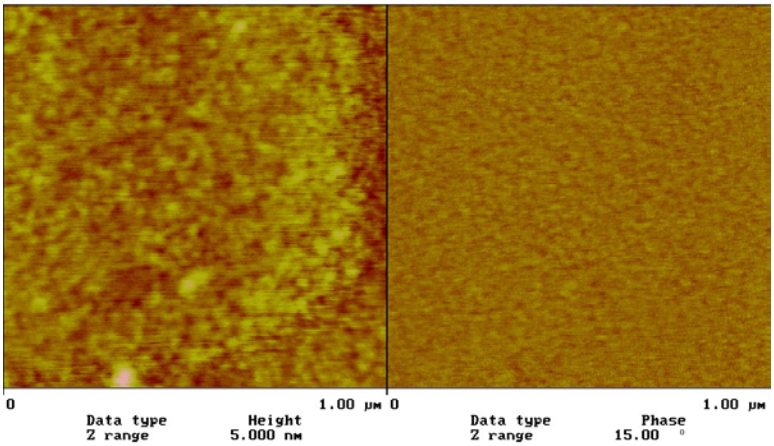

Figure 4.14: AFM height (left) and phase (right) images of an Ultem terminated (Ultem / PEI) ISAM film on silicon.

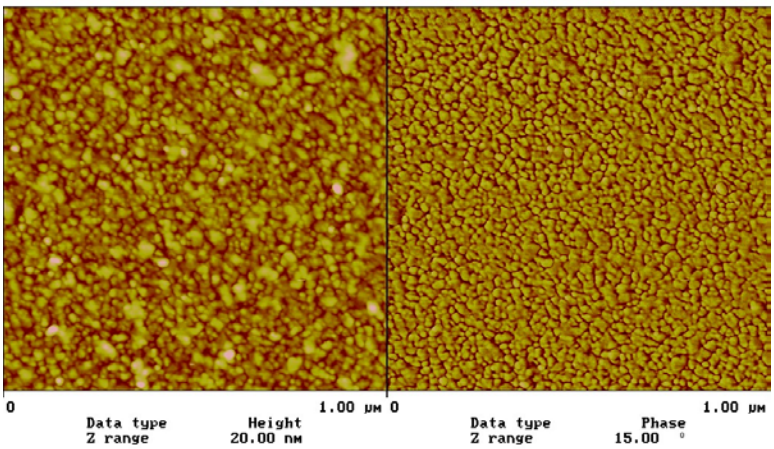

Figure 4.15: AFM height (left) and phase (right) images of a Laponite terminated (Ultem / PEI / Lap) ISAM film on silicon.

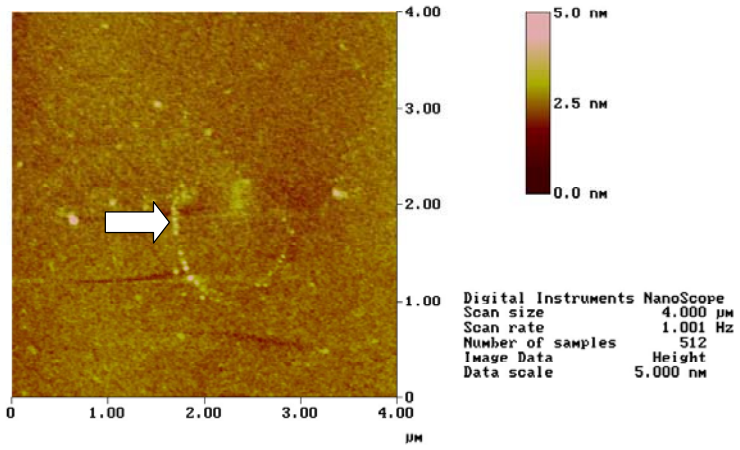

Figure 4.16: AFM height image of a Laponite terminated (Ultem / PEI / Lap) ISAM film showing a residual "crop circle" on the film on silicon.

3. Thermogravimetric analysis of polyethylenimine

TGA analysis of the PEI sample showed that the PEI sample lost 50 ± 0.5% of its mass. The lost mass corresponded directly to the reported amount of water present in the PEI sample. Degradation of the PEI polymer in air began at 300^{o}C.

D. Discussion

1. Overview of ISAM film performance

The Ultem based ISAM films showed significant corrosion resistance on aluminum coupons only when there was a significant oxide layer present. The performance of (Ultem / PEI) and (Ultem / PEI / Lap) films appears to be comparable. The formation of pits on the 2024_{sb} coupon during deposition of the (PAA / PAH) film is clearly attributable to the presence of Cl^- anions in the PAH solution. Not surprisingly, due to Cl^- anions, coupons covered with a (PAA / PAH) film exhibited poor corrosion resistance. It should be noted that the failure of the (PAA / PAH) films in this study does not reflect on the value of (PAA/PAH) films formed in literature for corrosion resistance.[51] In the cited source, all of the Cl^- anions were removed from the PAH solution using metallic sodium before deposition of the (PAA / PAH) films.

2. The effect of the oxide layer on Ultem based films

The presence of a thick, ~ 300 nm, oxide / hydroxide layer on the aluminum coupons appears to be critical to the successful performance of Ultem based ISAM films. The primary reason may be due to the dissolution of the aluminum and its oxide layer by OH^- anions during deposition. The Ultem, PEI, and Laponite solutions all have pHs above 8.0, where dissolution of aluminum begins. Diffusion of OH^- anions to the surface of the aluminum most likely slows as the ISAM film thickens. During deposition, there are two competing factors occurring on the surface of the aluminum: one is the dissolution of the aluminum or its oxide layer by OH^- anions, the other is the deposition of the polymer which slows the rate at which OH^- anions can reach the substrate's surface. If this second factor dominates, the ISAM film will eventually become so thick that OH^- diffusion through the film is effectively stopped. Solubility diagrams of aluminum are given in the Appendix.

Regardless of the oxide's thickness, some of the oxide will dissolve as the polymer is deposited. If a sufficiently thick oxide layer exists, however, the dissolution of the substrate will be slow enough to allow continued deposition of the polymer, which in turn slows the removal of the oxide layer even further. If only a native oxide of aluminum exists, the oxide layer will be quickly removed by the caustic ISAM solutions, exposing the underlying metallic aluminum. The bare aluminum, in turn will dissolve away faster than the build up of the polymer film. In this latter case, the polymer is being deposited on a continuingly disintegrating substrate; offering poor, if any corrosion protection, after deposition is completed.

3. The effect of surface roughness

Rough surfaces allow more contact between a substrate and a protective coating; so it was assumed that surface roughness would be beneficial for the films' adhesion. This study indicated otherwise. At the beginning of this study, it

was not known that surface roughness aids in the formation of pitting. After experimentation was completed, however, literature indicated that increased surface roughness promotes pitting in the presence of chloride ions.[55, 56, 57]

Ultem based ISAM films did demonstrate corrosion resistance on sandblasted samples, showing that the surface roughness of potential substrates, although a factor, is not critical to the successful performance of these films.

4. PEI and thermal imidization

The PEI used to make the Ultem based ISAM films survived the imidization process. The only mass lost driving TGA was due to water evaporation. PEI was expected to survive the imidization process, literature reports that the degradation temperature for PEI (Mw = 70 kg.mol^{-1}) is approximately 300^{o}C.[39]

PEI, despite its rich chemistry, will not react with the Ultem during the imidization process.[58] The effect of PEI on the resulting corrosion resistant film is unknown.

E. Conclusion

In conclusion, Ultem based ISAM films demonstrated corrosion resistance on 2024-T3 Al alloys, but only if there is a significant layer of surface oxide present. (PAA / PAH) films may offer some corrosion resistance, but these films' corrosion resistance is severely hampered by the presence of Cl^- in the PAH solution. Surface roughness promotes pitting on ISAM covered 2024-T3 Al substrates. Platelets of

[55] Wu, Tair I. "Effect of Surface Finish on the Corrosion Behavior of Commercial 7075 Al Alloy." Scripta Metallurgica et Materialia. v27, n7, p875. Oct 1992.

[56] Wu, Tair I; Wu, Jiann Kuo. "Effects of Surface Condition and Metallurgical Practice on the Corrosion Behavior of AA 7075 Aluminum Alloy." Corrosion Prevention and Control. v43, n1, p21. Feb 1996.

[57] Sasaki, K; Burstein, G.T. "The Generation of Surface Roughness During Slurry Erosion-Corrosion and its Effect on the Pitting Potential." Corrosion Science. v38, n12, p2111, 1996.

[58] Private communication with Professor J McGrath, Chemistry, Virginia Tech.

Laponite RD® were successfully incorporated into a working corrosion resistant ISAM film.

CHAPTER 5: CONCLUDING REMARKS

A. Final Conclusions

The ISAM process for a (PDDA / Mont) system was observed using AFM. Individual platelets of montmorillonite were found to be quite flexible and readily overlapped on another. Solution concentrations of clay above 0.02 w% lead to a break down of the ISAM process. When the ISAM process breaks down, clay platelets began to deposit upon one another rather than repel each other via electrostatic repulsion. As a result, mounds of clay form on the surface of the substrate rather than a uniform monolayer of clay. Ultrasonic agitation can be used to remove loosely bound clay platelets from the surface of the substrate. By using solution concentrations of clay above 0.02 w% in conjunction with ultrasonic cleaning a monolayer of clay platelets can be deposited on a mica substrate in ≤ 20 seconds.

The Tg of dried HPDDA was measured to be $231 \pm 5\ ^{o}C$. The degradation temperature of dried HPDDA in air was $275 \pm 5\ ^{o}C$. Spherulites of PDDA were created serendipitously on a silicon wafer and observed using AFM.

Silicon normally takes on a negative charge in aqueous solutions. It was found that ultrasonic cleaning of silicon may create circular regions of positive charge on the silicon's surface. It is hypothesized that ultrasonic cleaning creates bubbles on the surface of silicon; the presence of these bubbles reverses the surface charge of silicon by an unknown mechanism. PDDA and Laponite RD® can be used to form circular patterns on the surface ultrasonically cleaned silicon.

Salt spray testing has demonstrated that Ultem-based ISAM films can offer corrosion resistance to 2024-T3 Al substrates. A substantially thick (~300 nm) layer of aluminum oxide / hydroxide must exist on the substrate's surface in order for the Ultam-based ISAM films to offer any corrosion resistance. Nanoparticles of Laponite RD® were used to reinforce Ultem based ISAM films to form a nacre-like

nanolaminate. The incorporation of Laponite RD® into Ultem based ISAM films did not dramatically affect the ISAM films' corrosion performance.

B. Recommendations for Future Work

If work with Ultem based coatings is continued it is recommended that Ultem be mixed directly into a solution of Laponite rather than TPA. Laponite solutions are naturally basic, which may prevent the hydrolysis of the Ultem polymer chains when the Ultem is mixed into solution. During deposition the Ultem and Laponite will saturate the substrate together. By mixing the Ultem and Laponite solutions together, the use of mildly toxic TPA will be avoided; the volume fraction of Laponite in the film will probably be maximized and only two, rather than three, solutions will be used during deposition. A commercially available substitute for the Ultem-type salt should be found, however. The Ultem-type salt is not commercially available, extremely time consuming to synthesize, and supplies of the Ultem are severely limited.

Future ISAM corrosion resistant coatings should incorporate a mechanism to passivate the surface of the aluminum even if the film itself is damaged. One possibility is to use polyaniline in ISAM films. Polyaniline films have demonstrated corrosion resistance that extends even to damaged sections of film and have been utilized in commercially available corrosion resistant coatings like CORRPASSIV™.[59] Polyaniline can also be charged in aqueous solutions and was (until recently) commercially available in a water soluble form.

The ideal ISAM based corrosion coating would be a polyimide / polyaniline or polyamide / polyaniline system. The polyimide or polyamide would provide hydrophobicity, mechanical durability, and some corrosion resistance to the ISAM film, while the polyaniline would passivate the substrate even when the film is damaged. The incorporation of Laponite RD® into such a film is optional.

[59] Wessling, B. and Posdorfer, J. Synthetic Metals. v102, p1400, 1999.

Characterization of these ISAM films should be done using ellipsometry and electrochemical impedance spectroscopy measurements. Thicker films should be produced to test the limits of the corrosion protection offered by ISAM films. Obviously, all corrosion tests should be performed on smooth substrates with a thick oxide layer.

Finally, ISAM films have demonstrated their ability to adhere well to potassium aluminum silicates like mica. Therefore, it is highly probable that ISAM corrosion resistant films can be placed on top of conversion coatings that convert the surface of the aluminum to a potassium aluminum silicate. Environmentally these conversion coatings are relatively benign and do offer significant corrosion protection.[43] Future work may include improving these non-chromate coatings by adding an ISAM corrosion resistant coating on top of them.

APPENDIX A

Composition of 2024 Aluminum

w% / Alloy	Cr	Cu	Fe	Mg	Mn	Si	Ti	Zn	Total Others
Al 2024-T3	0.10	3.8-4.9	0.50	1.2-1.8	0.30-0.9	0.50	0.15	0.25	0.15

Nominal Isoelectric Points of Selected Ceramics[60]

Material	Nominal Composition	IEP
Quartz	SiO_2	2
Potassium feldspar	$K_2O{\cdot}Al_2O_3{\cdot}6SiO_2$	3-5
Kaolin(edges)	$Al_2O_3{\cdot}SiO_2{\cdot}2H_2O$	5-7
Alumina (Bayer process)	Al_2O_3	8-9

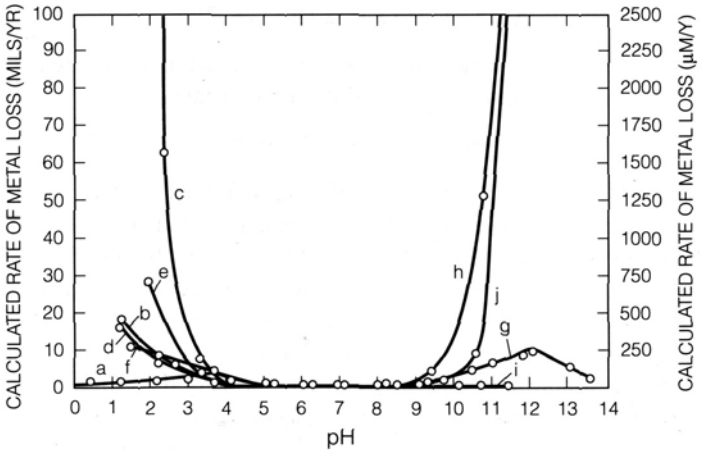

Effect of pH on corrosion rate of aluminum. A, acetic acid; b, hydrochloric acid; c, hydrofluoric acid; d, nitric acid; e, phosphoric acid; f, sulfuric acid; g, ammonium hydroxide; h, sodium carbonate; I, sodium disilicate; j, sodium hydroxide.[61]

[60] Patton, Temple C. Paint Flow and Pigment Dispersion. Wiley-Interscience, New York, 1979 and Errol Kelly, Errol G and Spottiswood, David J. Introduction to Mineral Processing. Wiley-Interscience, New York, 1982 reprinted in Reed, James S. Introduction to the Principles of Ceramic Processing. John Wiley & Sons. 1998.

[61] Hatch, J.E. Aluminum: Properties and Physical Metallurgy. ASM International. 1984 reprinted in Jones, Denny A. Principles and Prevention of Corrosion: 2nd ed. Simon & Schuster. 1992.

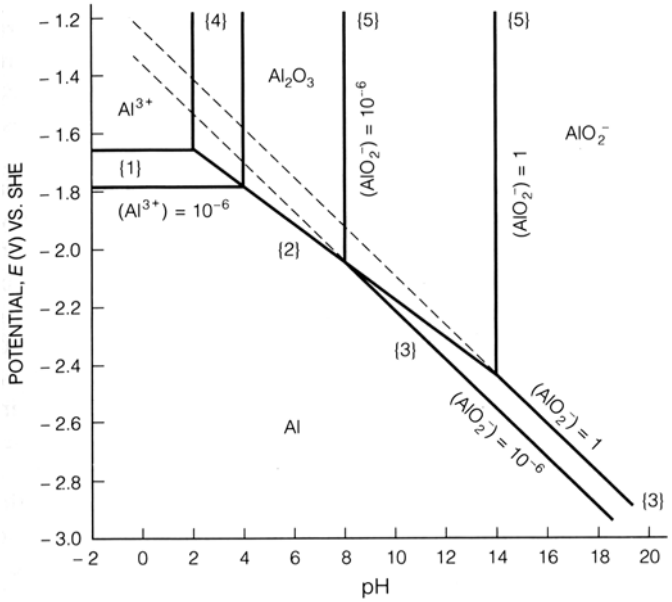

Potential/pH diagram showing equilibrium for the reaction

$Al + 2H_2O = AlO_2^- + 4H^+ + 3e^-$.[62]

Solubility of aluminum oxide and its hydrates[63]

Compound	Formula	pH on dissolution in water
Hydrargillite	$Al_2O_3 \cdot 3H_2O$	6.8
Bayerite	$Al_2O_3 \cdot 3H_2O$	6.7
Bohmite	γ-$Al_2O_3 \cdot H_2O$	6.1
Corundum	α-Al_2O_3	5.9
Amorphous hydroxide	$Al(OH)_3$	5.3

[62] Jones, Denny A. Principles and Prevention of Corrosion: 2nd ed. Simon & Schuster. 1992.

[63] Pourbaix, Marcel. Atlas of Electrochemical Equilibria in Aqueous Solutions. National Association of Corrosion Engineers. 1974.

Improved Manual Cleaning Procedure

1) Fill a clean 150 mL beaker with deionized water
2) Dip the substrate into the desired solution
3) Hold the substrate in the solution for the prescribed amount of time
4) Remove the substrate from the solution and pour half of the beaker out on one side of the substrate
5) Remove the substrate from the solution and pour half of the beaker out on the other side of the substrate
6) Refill the 150 mL beaker with deionized water
7) Repeat steps 4-5, for a total of two rinses
8) Refill the 150 mL beaker with deionized water
9) Put the substrate into the beaker and move the substrate around inside the beaker
10) Remove the substrate from the beaker
11) Pour the half contents of the beaker onto one side of the substrate
12) Pour the remaining contents of the beaker onto the other side the substrate
13) Repeat steps 8-12 twice, for a total of three rinses
14) Repeat steps 1-13 until deposition is completed.
15) Blow dry the substrate with N_2 gas

ISAM glassware cleaning procedure

1) A plastic washbasin is filled with tap water.
2) Sparkleen® cleaning soap from Fisher Scientific is added to the tap water.
3) Glassware is placed into the washbasin.
4) Glassware is vigorously cleaned using a pipe cleaner.
5) Glassware is flushed with tap water for approximately 10 seconds.
6) Glassware is filled with tap water and emptied at least 3 times.
7) Glassware is filled with deionized water and emptied at least 3 times.
8) Glassware is set aside to dry.

Deposition Sequences used to Produce Maze Morphologies

1) ((20.00 w% LPDDA, 60 s [US 10 s]) (0.20 w% Mont 10 s [US 10 s]))$_1$ on mica
2) ((20.00 w% HPDDA, 10 s [US 10 s]) (0.20 w% Mont 10 s [US 10 s]))$_1$ on mica
3) ((4.00 w% HPDDA, 4 s [US 10 s]) (0.10 w% Mont 4 s [US 10 s]))$_{1.5}$ on mica
4) ((4.00 w% HPDDA, 10 s [US 10 s]) (0.20 w% Mont 10 s [US 10 s]))$_2$ on mica
5) ((4.00 w% HPDDA, 10 s [US 10 s]) (0.20 w% Mont 30 s [US 10 s]))$_2$ on mica
6) ((4.00 w% HPDDA, 10 s [US 10 s]) (0.20 w% Mont 60 s [US 10 s]))$_{2.5}$ on mica
7) ((4.00 w% HPDDA, 10 s [US 10 s]))$_1$ on mica
8) ((4.00 w% HPDDA, 10 s [US 10 s]) (0.20 w% Mont 60 s [US 10 s]))$_1$ on mica
9) ((4.00 w% HPDDA, 10 s [US 10 s]) (0.20 w% Mont 60 s [US 10 s]))$_1$ on mica
10) ((3.00 w% HPDDA, 60 s [US 10 s]) (0.20 w% Mont 60 s [US 10 s]))$_{5.5}$ on mica
11) ((3.00 w% HPDDA, ph=7.5, 60 s [US 10 s])$_1$ on mica
12) ((4.00 w% HPDDA, 60 s [US 10 s]) (0.20 w% Mont 60 s [US 10 s]))$_{1.5}$ on mica
13) ((4.00 w% HPDDA, 10 s [US 10 s]) (0.20 w% Mont 60 s [US 10 s]))$_2$ on mica
14) ((4.00 w% HPDDA, 10 s [US 10 s]) (0.20 w% Mont 60 s [US 10 s]))$_3$ on mica
15) ((4.00 w% HPDDA, 10 s [US 10 s]) (0.20 w% Mont 60 s [US 10 s]))$_{3.5}$ on mica
16) ((4.00 w% HPDDA, 10 s [US 10 s]) (0.20 w% Mont 60 s [US 10 s]))$_{3.5}$ on mica
17) (5.00 w% HPDDA, 10 s [US 10 s])$_1$ on Si
18) (5.00 w% HPDDA, 10 s [US 10 s])$_1$ on Si
19) (5.00 w% HPDDA, 10 s [US 10 s])$_1$ on Si
20) ((4.00 w% HPDDA, ph=8.6, 10 s [US 10 s]) (0.20 w% Mont 60 s [US 10 s]))$_4$ on Si
21) (5.00 w% HPDDA, 10 s [US 10 s])$_1$ on mica
22) (5.00 w% LPDDA, ph=8.0, 10 s [US 10 s])$_1$ on mica
23) (5.00 w% LPDDA, ph=8.0, 10 s [US 10 s])$_1$ on mica
24) (4.00 w% HPDDA, ph=8.6, 10 s [US 10 s])$_1$ on mica
25) (4.00 w% HPDDA, ph=8.6, 10 s [US 10 s])$_1$ on mica
26) (5.00 w% LPDDA, ph=8.0, 60 s [US 10 s])$_1$ on Si
27) (4.00 w% HPDDA, ph=8.6, 10 s [US 10 s])$_1$ on Si
28) (5.00 w% LPDDA, 60 s [US 30 s])$_1$ on mica
29) (5.00 w% LPDDA, 60 s [US 30 s])$_3$ (0.20 w% Mont 60 s [US 10 s]) (20.00 w% HPDDA, 60 s [US 10 s]))$_1$ on Si

Deposition Sequences used to Produce Island Morphologies

1) ((2.00 w% HPDDA, 10 s [US 10 s]) (0.20 w% Mont 10 s [US 10 s]))$_{3.5}$ on mica
2) (5.00 w% LPDDA, ph=8.0, 10 s [US 10 s])$_1$ on mica
3) (5.00 w% LPDDA, 60 s [US 30 s])$_1$ on mica

Deposition Sequences used to Produce Needle Morphologies

1) ((20.00 w% LPDDA, 3600 s [US 10 s]) (0.20 w% Mont 10 s [US 10 s]))$_{1.5}$ on mica
2) ((0.02 w% LPDDA, 10 s [US 10 s]) (0.20 w% Mont 10 s [US 10 s]) (20.00 w% LPDDA 10 s [US 10 s]))$_1$ on mica
3) (20.00 w% HPDDA, 10 s [US 10 s])$_1$ on mica
4) (20.00 w% LPDDA, 60 s [US 10 s]) ((20.00 w% LPDDA, 60 s [US 10 s]) (0.20 w% Mont 60 s [US 10 s])$_2$)$_1$ on Si

Deposition Sequences used to Produce Haystack Morphologies

1) ((5.00 w% HPDDA, 5 s [US 10 s]))$_1$ on mica
2) ((20.00 w% LPDDA, 3600 s [US 10 s]) (0.20 w% Mont 10 s [US 10 s]))$_{1.5}$ on mica
3) ((20.00 w% LPDDA, 60 s [US 10 s]) (0.20 w% Mont 10 s [US 10 s]))$_{1.5}$ on mica
4) ((0.02 w% LPDDA, 10 s [US 10 s]) (0.20 w% Mont 10 s [US 10 s]) (20.00 w% LPDDA 10 s [US 10 s]))$_1$ on mica
5) ((20.00 w% LPDDA, 10 s [US 10 s]) (0.20 w% Mont 10 s [US 10 s])$_2$ (20.00 w% LPDDA 10 s [US 10 s]))$_1$ on mica
6) (20.00 w% HPDDA, 10 s [US 10 s])$_1$ on mica
7) (5.00 w% LPDDA, 60 s [US 30 s])$_3$ (0.20 w% Mont, 60 s [US 10 s]) (20.00 w% LPDDA, 60 s [US 10 s]))$_1$ on Si
8) ((5.00 w% LPDDA, 60 s [US 10 s])$_2$ (10.00 w% LPDDA, 60 s [US 10 s]))$_1$ ((10.00 w% HPDDA,10 s [US 10 s]) (0.20 w% Mont, 60 s [US 10 s]))$_2$ on Si
9) (20.00 w% LPDDA, 60 s [US 10 s])$_1$ ((20.00 w% LPDDA, 60 s [US 10 s]) (0.20 w% Mont 60 s [US 10 s])$_2$ on Si

Deposition Sequences used to Produce Rod Morphologies

1) (5.00 w% HPDDA, 5 s [US 10 s])$_1$ on mica
2) ((5.00 w% HPDDA, 5 s [US 5 s]) (0.20 w% Mont 5 s [US 5 s]))$_{1.5}$ on mica
3) ((20.00 w% LPDDA, 10 s [US 10 s]) (0.20 w% Mont 10 s [US 10 s]))$_{1.5}$ on mica
4) (20.00 w% LPDDA, 10 s [US 10 s])$_1$ on mica
5) ((20.00 w% LPDDA, 10 s [US 10 s]) (0.20 w% Mont 10 s [US 10 s])$_2$)$_3$ on mica
6) (5.00 w% LPDDA, 60 s [US 30 s])$_3$ (0.20 w% Mont, 60 s [US 10 s]) (20.00 w% LPDDA, 60 s [US 10 s]))$_1$ on Si
7) (5.00 w% LPDDA, 60 s [US 10 s])$_3$ ((0.20 w% Mont, 60 s [US 10 s]) (20.00 w% LPDDA, 60 s [US 10 s]))$_2$ on Si
8) (5.00 w% LPDDA, 60 s [US 10 s])$_2$ (10.00 w% LPDDA, 60 s [US 10 s])$_1$ ((10.00 w% HPDDA,10 s [US 10 s]) (0.20 w% Mont, 60 s [US 10 s]))$_2$ on Si
9) (20.00 w% LPDDA, 60 s [US 10 s])$_1$ ((20.00 w% LPDDA, 60 s [US 10 s]) (0.20 w% Mont 60 s [US 10 s]))$_2$ on Si

Deposition Sequences used to Produce Spherulites

10) (5.00 w% LPDDA, 60 s [US 10 s])$_3$ ((0.20 w% Mont, 60 s [US 10 s]) (20.00 w% LPDDA, 60 s [US 10 s]))$_2$ on Si

Deposition Sequences used to Produce Montmorillonite Patterns

1) ((0.02 w% PDDA, 10 s [Norm]) (0.02 w% Mont 10 s [Norm]))$_1$ on mica (Rows)
2) ((0.02 w% PDDA, 10 s [Norm]) (2.95 w% Closite 10 s [Norm]))$_1$ on mica (Stacks)

Deposition Sequences used to Produce Crop Circles

1) ((4.00 w% HPDDA, 10 s [US 10 s]) (0.20 w% Mont 60 s [US 10 s]))$_4$ on Si
2) ((4.00 w% HPDDA, 10 s [US 10 s]) (0.20 w% Mont 60 s [US 10 s]))$_1$ on Si
3) (4.00 w% HPDDA, 10 s [US 10 s]) (0.20 w% Mont 60 s [US 10 s]))$_2$ on Si
4) (5.00 w% LPDDA, 60 s [US 10 s])$_1$ on Si
5) (5.00 w% LPDDA, 60 s [US 30 s])$_1$ on Si
6) (2.00 w% LPDDA, pH=8.2, 60 s [Norm])$_4$ on Si
7) (5.00 w% LPDDA, 60 s [US 10 s])$_1$ on Si
8) (4.00 w% HPDDA, 60s [Norm])$_1$ on Si (Repeatable formation of crop circles)
9) (4.00 w% HPDDA, 60s [US])$_1$ on Si (Repeatable formation of crop circles)

Deposition Sequence used to Produce Stonehenges

1) (0.02 w% Lap + 0.02 w% PSS, 30 s [Norm])$_1$ on Si

VITAE

Matthew Gordon is originally from Frederick, MD. He received his B.S. in Materials Science and Engineering at Virginia Tech in the summer of 2000. While an undergraduate, he worked with Dr. Bill Curtin on ceramic matrix composites and on contract proposals with Luna Innovations. Matthew completed his M.S. in Materials Science and Engineering at Virginia Tech in the summer of 2001. Most of his extracurricular activities at Virginia Tech have been centered around a student orientated church, New Life Campus Fellowship. He plans to attend the University of Washington in Seattle where he will study Materials Science and Engineering with a concentration in biomimetics. His primary research interests are biomimetics, ballistic armor, and biodegradable materials.